DRFC/CAD

EUR-CEA-FC-1619

Dynamic Modelling of Tearing Mode Stabilization by RF Current Drive

G Giruzzi, M Zabiego, T A Gianakon, X Garbet, A Cardinali, S Bernabei

Juin 1998

DYNAMIC MODELLING OF TEARING MODE STABILIZATION BY RF CURRENT DRIVE

G. Giruzzi, M. Zabiégo, T.A. Gianakon, X. Garbet

Association EURATOM-CEA sur la Fusion,
Département de Recherches sur la Fusion Contrôlée, CEA/Cadarache,
13108 St. Paul-lez-Durance (FRANCE)

A. Cardinali

Associazione EURATOM-ENEA sulla Fusione
Centro Ricerche Energia Frascati, C.P. 65
00044 Frascati (ITALY)

S. Bernabei

Plasma Physics Laboratory
Princeton University
Princeton, NJ 08543 (USA)

Abstract

The theory of tearing mode stabilization in toroidal plasmas by RF-driven currents that are modulated in phase with the island rotation is investigated. A time scale analysis of the phenomena involved indicates that transient effects, such as finite time response of the driven currents, island rotation during the power pulses, and the inductive response of the plasma, are intrinsically important. A dynamic model of such effects is developed, based on a 3-D Fokker-Planck code coupled to both the electric field diffusion and the island evolution equations. Extensive applications to both Electron Cyclotron and Lower Hybrid current drive in ITER are presented.

1. INTRODUCTION

Tearing modes are one of the major causes of degradation of plasma stability and confinement in tokamaks. They are resonant instabilities, localized around flux surfaces characterized by rational values of the safety factor q, which manifest themselves by the formation of magnetic islands. As these islands grow in size non-linearly, the modes may lead to violent disruptions, a particularly dangerous phenomenon for a high-current tokamak reactor. A special class of these MHD instabilities, neoclassical tearing modes, are observed to limit the performance of high-β tokamak experiments [1-5] and are expected to set the actual β limit in a fusion reactor [6,7] well below the Troyon limit [8] (β is the ratio of the plasma to the magnetic pressure). Although practical recipes of plasma operation have been found in order to avoid the most dangerous of these instabilities, such methods do not necessarily work in the most interesting, fusion relevant, regimes. For instance, current density profiles which are known to be stable against tearing modes, may not be those associated with the highest achievable confinement times or may not be suitable for long-pulse discharges. Furthermore, neoclassical modes, being influenced by pressure effects, cannot be controlled through the safety factor profile only. Ideally, a method of controlling tearing modes is needed which, to a large extent, is independent of the global plasma parameters, acts locally at resonant surfaces, and prevents or stops the non-linear growth of the mode. The interaction of radio-frequency waves with the plasma may well take place locally, and has been proposed by a number of authors as an effective means of controlling the tearing modes [9-24]. Three different methods have been suggested [12]:

i) prevention of the mode growth by local modification of the current density gradient, by flattening the current profile just inside the resonant surface [17];

ii) stabilization of the mode by local heating inside the magnetic islands [9,10]. This causes a current perturbation owing to the enhancement of the electrical conductivity and, in turn, a magnetic field which tends to cancel the magnetic perturbation of the mode;

iii) generation of a current perturbation directly inside the island by non-inductive current drive [11-14].

Both the second and the third method are more efficient if the wave-plasma interaction takes place inside the islands, which requires not only radial, but also poloidal and toroidal current localization. Since the islands typically rotate with frequencies between hundreds of Hz and tens of kHz, these processes are optimized by modulating the wave power in phase with the island rotation. If such RF modulation is possible, these latter two methods are expected to be significantly more efficient than the first one [18]. Partial or total stabilization of m = 2 tearing modes by Electron Cyclotron (EC) heating has been experimentally demonstrated [25-28], including the beneficial effect of power modulations [29,30]. On the other hand, an experimental proof of the direct current drive method is still lacking, although theoretical comparisons of island heating and current drive effects [12-14,17,22] predict that direct current drive should be intrinsically superior, besides the obvious effect that current drive also provides local heating.

Here, the potentially most efficient method, i.e., direct current drive in the island region, is investigated. Since power modulations are expected to be an important factor of optimization, and they are well within the possibilities of the present-day wave source technology, up to tens of kHz, it is important to study the impact of time-dependent phenomena on the stabilization efficiency. This problem has not been fully investigated so far, which motivates the present work. At least three basic phenomena of this type can be identified. First, non-inductive current drive is not an instantaneous effect [31]. The driven current is due to a superthermal electron tail that builds up as a

consequence of velocity-space diffusion induced by the RF waves. This takes at least a typical kinetic time, which can easily be of the same order as the island rotation period. No simple expression exists for the current driven in this transient regime and using the familiar steady-state current drive efficiency is, of course, generally incorrect. A second effect is related to the inductive response of the plasma. In fact, the previously mentioned kinetic time should be regarded only as a turn-on time of the current source, which does not coincide with the turn-on time of the power, which can well be considered as instantaneous. The plasma response to this current source is an induced electric field opposing the current perturbation, as observed in any current drive experiment [31] (back emf, electro-motive force). On short time scales, this electric field provides the stabilizing mechanism, but in general this field must be evaluated self-consistently with the fast electron distribution function. The third effect is a consequence of the previous two: since the stabilizing field cannot be turned on and off instantaneously during the power modulations, but at the same time the island rotates, it is practically impossible to concentrate the driven current at the island O-point , and therefore the stabilization efficiency will generally be a function of the island rotation frequency. The development of a simple model which allows a proper treatment of the combination of these dynamic effects appears to be a difficult task. For this reason, here the problem is addressed by numerically solving the appropriate time-dependent kinetic equation for the electron distribution function. In order to correctly evaluate the transient current drive efficiency, this equation must be two-dimensional in velocity space ($v_{||}$, $v_{\perp}$, where parallel and perpendicular subscripts refer to the direction of the equilibrium magnetic field). Since localization of the driven current is expected to be important, this equation should also be, at least, one-dimensional in real space (the magnetic flux co-ordinate). Incidentally, it should be noted that, if radial diffusion of the driven current is an issue, the only way of evaluating this effect is through the kinetic equation itself, since the current is carried by the tail electrons. Note that this

model however does not self-consistently handle the geometry of the island. Owing to the fact that the back emf plays a central role, the kinetic equation must be coupled to an evolution equation for the induced electric field. This procedure yields the appropriate, time-dependent source term to be inserted into a standard island evolution equation [32], or into a full non-linear MHD evolution code, possibly including neo-classical effects [33].

In this paper, a dynamic model of this type, based on a 3-D kinetic equation, is introduced, in order to evaluate the impact of time-dependent effects on the stabilization efficiency, with the aim of providing reliable estimates of: i) the power required for this task in tokamak reactors; ii) the time necessary for a substantial reduction of the island size; iii) the minimum island width compatible with realistic RF waves parameters. Ideally, the power should be a reasonably small fraction of the total additional heating power; the time should be shorter than the typical island growth time; the minimum island width should be small enough to cause an acceptable loss in plasma confinement. The outline of the paper is the following: The different time scales involved in the problem are discussed in Sec. 2. The dynamic model is described in Sec. 3. An application to the stabilization of an m = 2 mode in ITER is then presented. As is known, Electron Cyclotron Current Drive (ECCD) is the leading candidate for this function in ITER. However, the ECCD efficiency in the outer part of the plasma (where the most dangerous modes are) is expected to be low, because of trapped electron effects [34]. Therefore, the option of using Lower Hybrid (LH) waves is also considered, and a comparison of the two systems is made. The propagation properties and the localization of the absorption for the two waves are discussed in Sec. 4. Dynamic effects are evaluated for different values of the modulation frequency and are discussed in Sec. 5. Solutions of the island evolution equation in various cases are presented in Sec. 6. The results are discussed, and conclusions are drawn in Sec. 7.

2. TIME SCALES OF A NON-INDUCTIVE CURRENT SOURCE

The non-inductive current drive process results from the balance of quasilinear diffusion in velocity space, associated with wave-particle interaction, and Coulomb collisions [31]. The wave-particle interaction has to be asymmetric in the parallel velocity $v_{||}$, in order to create a corresponding asymmetry in the electron distribution function. Because of the resonant nature of the interaction, this is usually obtained by means of asymmetric $k_{||}$ spectra, where $k_{||}$ is the projection of the wave vector on the tokamak magnetic field. Since Coulomb collisions tend to isotropize the electron distribution, the driven current is optimized for poorly collisional resonant electrons, i.e., superthermal ones. A significant fast electron tail is generated if quasilinear diffusion dominates over Coulomb collisions. The basic time scale of the phenomenon is $\tau_D \sim (\Delta v)^2/D_{rf}$, where Δv is the typical velocity range where the interaction takes place and D_{rf} is the quasilinear diffusion coefficient, that is proportional to the RF wave power. This power-dependent diffusion time is by no means a current rise time. In fact, the non-inductive current originates from three distinct processes [31]:

i) Wave-electron parallel momentum exchange: this is the most direct phenomenon, that takes place on the quasilinear time scale τ_D, but requires waves with a high longitudinal component, inducing parallel diffusion in velocity space (as, e.g., LH waves). In contrast, in the case of ECCD, the velocity space diffusion takes place predominantly in the perpendicular direction, and negligible parallel current is generated by this mechanism.

ii) Selective electron trapping: on flux surfaces characterized by a significant magnetic well, perpendicular diffusion causes the resonant electrons to become trapped, which implies a net loss of parallel current (because the interaction is asymmetric in $v_{||}$). This reverse current, known as Ohkawa current [35], can rise on time scales of the order of τ_D, but it is generally small.

iii) Asymmetric collisionality: because of the asymmetric energy exchange between waves and electrons, the $1/v^3$ dependence of the collision frequency produces an asymmetric collision rate, that is responsible for the so-called Fisch-Boozer current [36]. This is generally the largest contribution to the total non-inductive current. Even in the case of parallel diffusion (as due, e.g., to LH waves), this collisional effect dominates the current directly driven by momentum exchange, more precisely by a factor of three [36].

As a consequence, the relevant time scale for the build-up of the electron tail is actually determined by the effective collision time of the resonant electrons $\tau_c(v)= \nu^{-1}$, where $\nu = (5+Z)/(\tau_e(v/v_{th})^3)$ is the current destruction rate defined in Ref. [36], $\tau_e = (m_e^2 v_{th}^3)/(2\pi e^4 \Lambda n_e)$ is the thermal electron collision time, $v_{th} = (T_e/m_e)^{1/2}$, Λ is the Coulomb logarithm, Z is the effective ion charge number, and e, m_e, n_e, T_e are the electron charge, mass, density and temperature, respectively. If inductance effects are neglected, and if v is interpreted as an average resonant velocity, this is the actual rise time of the non-inductive current I_{rf}. Figure 1 illustrates the time evolution of the driven current, computed by means of a 3-D Fokker-Planck code [37], for LHCD (a) and ECCD (b), respectively. The parameters used in these simulations are appropriate for the control of an m = 2 tearing mode in a standard ITER equilibrium [38], and will be given in Sec. 4. In both cases, the absorbed RF power is of the order of 50 MW. The two curves display both qualitative and quantitative differences, which can be easily understood. First of all, the LH-driven current does not change sign, since for Landau-damped waves the current is driven by parallel diffusion, inducing electron de-trapping rather than trapping: thus, the Ohkawa current has the same sign as the Fisch-Boozer current. An additional difference in the current drive efficiency of a factor 4/3 in favour of LH waves is due to direct parallel momentum exchange between wave and electrons [36]. The average resonant velocities are different in the two cases, for the specific wave frequencies and $k_{||}$ spectra chosen, i.e., $v_{||}/v_{th} \approx 4.7$ and 3.2 for LH and

EC waves, respectively. This explains the difference in time scales, as well as part of the difference in the total driven current. The remaining difference is due to trapping effects, which are negligible in the case of LH waves and significant for EC waves.

Now, the characteristic time τ_c, which turns out to be in the millisecond range, should be regarded as a turn-on time of the current source, rather than of the current itself. As any electric circuit, the plasma reacts to the current ramp by an induced electric field, that, on a short time scale, exactly cancels the non-inductive current, keeping the current density profile constant [31]. Later on, this induced electric field diffuses away, and the current density profile is effectively modified. This happens on a time scale related to the resistive time $\tau_R = a^2\mu_0\sigma$, where a is the plasma minor radius, μ_0 is the magnetic permeability of free space, and σ is the electrical conductivity. If $\Delta\rho$ is the normalized radial width of the current source (ρ being defined as $\sqrt{\psi}$, where ψ is the normalized magnetic flux), this time is of order $\tau_\rho = (\Delta\rho)^2\tau_R$, which, for hot plasmas, usually exceeds τ_c. For instance, for ITER parameters [38], $\rho \approx 0.8$, $\Delta\rho \approx 0.1$, it is found that $\tau_\rho/\tau_c \approx 10^4$. This means that the driven current cannot be modulated at frequencies in the 0.1 - 10 kHz range, but, at best, at a frequency $1/\tau_\rho$. What can be rapidly modulated is the induced electric field, with a maximum frequency $1/\tau_c$. However, this circumstance does not prevent the mode stabilization process, since, in the island non-linear evolution [32], the plasma response is governed by Ohm's law $\vec{E} + \vec{v} \times \vec{B} = \eta\vec{J}$, which does not distinguish between a current and an electric field perturbation of opposite signs.

In conclusion, the relevant time scale for this problem is the resonant electron collision time τ_c, which is of the order of the millisecond, i.e., in the range of the island rotation period. On this basis, a reduction of the stabilization efficiency can be anticipated for high island rotation frequency, since the induced electric field cannot be turned on and off in a time much shorter than the rotation period. The time τ_D is related to the rise of the Ohkawa current in the case of ECCD, and represents a sort of delay to

the appearance of an induced electric field of the right sign; it has little relevance in the case of LHCD. If the time needed to substantially reduce the mode amplitude becomes of the order of τ_ρ, then the current density profile is modified, current diffusion starts to play a role, and changes of the stability index Δ' [32], as well as of the position of the resonant surface, are to be expected. In the most general case, a model capable of evaluating the time-dependent current source, the induced electric field and the current profile evolution simultaneously is necessary. Such a model is described in the next section.

3. BASIC EQUATIONS OF THE DYNAMIC MODEL

A computational model describing the process of tearing mode stabilization by RF current drive would be a very complex one, requiring the coupling of several codes. In principle, a magnetic equilibrium perturbed by the rotating islands would be needed. The wave propagation should be evaluated in this equilibrium, and would be modified by the island evolution itself. The RF current source would have to be computed by means of a 3-D Fokker-Planck code, bounce-averaged over the electron orbits in the perturbed magnetic configuration and would have to include fast electron diffusion. The induced electric field resulting from Faraday's and Ampère's equations then provides the stabilizing term to be inserted into a 3-D non-linear MHD code for the evolution of the tearing modes, which yields an updated equilibrium to continue the time iterations. Since the waves also heat the plasma as they drive currents, the MHD and RF equations must be consistently solved with the heat transport equation, which is an essential step in order to correctly evolve the pressure, for simulations of neoclassical tearing modes. Because of the wide range of time scales of the processes

and the complexity of each code involved, a full solution of the problem appears prohibitive. Here, only a part of this ambitious task is accomplished, although a significant one: in order to evaluate the modulation effect correctly, the 3-D Fokker-Planck equation is coupled to an equation for the electric field diffusion. This provides the stabilizing term to be used in a simple equation for the time evolution of the island width [32], or in a full 3-D evolution code for the MHD modes. The main simplifications adopted are the following:

i) Only stabilization by the effect of non-inductive current is considered, and the heating effect is neglected, which allows to work with an electron temperature profile constant in time. This assumption is justified by the fact that the direct current drive effect is expected to be much stronger than the heating effect [12-14,17,22].

ii) The wave propagation is evaluated in a magnetic equilibrium not perturbed by the modes. In fact, the propagation of EC waves, which are high-frequency waves, is known to be weakly affected by the detailed structure of the magnetic equilibrium; for LH waves this is less evident, but it has been demonstrated in a specific work [39].

iii) The kinetic equation is bounce-averaged over the electron orbits in the unperturbed equilibrium. This is perhaps the most critical assumption of the model, and it is justified in regimes characterized by weak quasilinear effects on the RF current drive efficiency, as is the case for reactor relevant parameters. In general, quasilinear effects will be enhanced when the wave power is absorbed well inside a magnetic island, owing to the fact that the power is distributed on smaller flux surfaces. This means that enhanced quasilinear effects could possibly affect the stabilization process in the phase in which the island width w is larger than the power deposition width Δr. However, such effects are expected to be very weak for ITER-like parameters, as used in the present work.

iv) The use of an island width evolution equation, rather than a full 3-D evolution code, should be considered as a simple way to discuss the principal point of this work, i.e.,

the role of dynamic effects. Use of the correct stabilizing term computed here in a 3-D non-linear MHD code [33] is also possible, and preliminary results have been presented elsewhere [40].

3.1. RF Model

An explicit equation for the time evolution of the driven current source, including radial diffusion and a parallel electric field, is not available. However, the current source can be directly evaluated from the electron distribution function f(p, ρ, t), where p is the electron momentum, ρ the normalized radial co-ordinate and t the time, by solving the appropriate bounce-averaged kinetic equation

$$\frac{\partial f}{\partial t} = \hat{C}(f) + eE_{\parallel}\frac{\partial f}{\partial p_{\parallel}} + \frac{\partial}{\partial \vec{p}} \cdot \boldsymbol{D}_{rf} \cdot \frac{\partial f}{\partial \vec{p}} + \frac{1}{\rho}\frac{\partial}{\partial \rho}\rho D_r \frac{\partial f}{\partial \rho} \qquad (1)$$

where $\hat{C}$ is the Coulomb collision operator, $p_{\parallel}$, $E_{\parallel}$ are the parallel components of the electron momentum and of the electric field with respect to the magnetic field, $\mathbf{D_{rf}}$ is the quasilinear diffusion coefficient for the RF waves, and D_r is the (normalized) radial diffusion coefficient, generally related to electrostatic and magnetic turbulence. Detailed expressions of the different terms can be found in several publications, e.g., Ref. [41, 37]. In order to describe correctly the current drive process, this equation must be 2-dimensional in momentum space. Several numerical codes exist that solve this equation for an electric field $E_{\parallel}(\rho)$ constant in time. However, in order to describe transient effects this is often a poor approximation. A relatively simple equation for $E_{\parallel}$ can be derived from Faraday's and Ampère's equations, by making the assumption that the electrical conductivity σ does not depend itself on the transient evolution of f, but only on the macroscopic parameters T_e and Z. This assumption is based on the fact that the kinetic time scale for the establishment of a stationary ohmic current, mainly carried by subthermal electrons, is much shorter than the corresponding time for non-inductive current, which is, in turn, carried by superthermal electrons. This can be checked by means of the Fokker-Planck code itself, and it is usually well verified. Moreover, it is

consistent with the approximation of neglecting the electron inertia in the MHD equations. With this assumption, the electric field diffusion equation is usually written as

$$\frac{\partial E_{\|}}{\partial t} = \frac{1}{\tau_R}\frac{1}{\rho}\frac{\partial}{\partial \rho}\rho\frac{\partial E_{\|}}{\partial \rho} - \frac{E_{\|}}{\sigma}\frac{\partial \sigma}{\partial t} - \frac{1}{\sigma}\frac{\partial J_{rf}}{\partial t} \qquad (2)$$

where J_{rf} is the purely RF part of the total current density J, i.e., $J_{rf} = J - \sigma E_{\|}$, and for σ a suitable expression of the neoclassical conductivity is used. Equation (1) is solved by a standard alternating direction implicit difference method, as described elsewhere [42]. At every time step Δt, the quantity J_{rf} is computed as

$$J_{rf}(\rho,t) = -e\int d^3\vec{p}\; v_{\|} f(\vec{p},\rho,t) - \sigma(\rho)E_{\|}(\rho,t-\Delta t) \qquad (3)$$

and it is inserted into Eq. (2), which is then solved by means of an implicit finite difference scheme, with initial condition $E_{\|} = E_{\|0} = V_{loop}/2\pi R_0$, where V_{loop} is the loop voltage and R_0 is the tokamak major radius. This procedure is not particularly time-consuming and yields the expected result: on a short time scale, the current density remains essentially constant, except for some weak oscillations in the first iterations, and a large electric field builds up in the region where the wave power is absorbed. Some examples of this behaviour will be shown in the next section. The main difficulty with this algorithm is the choice of the boundary condition at the plasma edge ($\rho = 1$). In general, this condition should be coupled with the evolution of the currents in the poloidal and vertical field coils, which in principle can be done, but adds a significant complication to the calculation. However, for the specific problem of tearing mode stabilization, the additional current driven is generally small, typically a few percent of the total plasma current. This allows to neglect the tokamak primary circuit reaction, and to assume a much simpler boundary condition, e.g., a constant $E_{\|} = E_{\|0}$. On the other hand, the boundary condition imposed at $\rho = 0$ is the standard one for cylindrical problems, i.e., $\partial E_{\|}/\partial\rho = 0$. Note that the kinetic evolution of the

electron distribution function is, in principle, influenced by the induced $E_{||}$, which tends to decelerate the fast electrons interacting with the waves. This is why, in general, the problem has to be solved self-consistently.

3.2. MHD stability model

Equations (1-3) are used to evaluate the appropriate perturbation δJ to the equilibrium current density in the Ohm's law. For times shorter than τ_ρ, this perturbation originates from the induced electric field, $\delta J = -\sigma(E_{||} - E_{||0})$, whereas later on it manifests itself as an actual perturbation to the current density profile, i.e., $\delta J = J - J_{eq}$. The perturbation is then inserted into the evolution equation for the island width w, which can be written as [22]

$$\frac{dw}{dt} = \frac{k_R}{\sigma\mu_0}\left[\Delta' + \Delta'_\beta + \Delta'_{CD}\right] \tag{4}$$

where k_R is a dimensionless numerical constant of order 1, and $\Delta'(w)$ is the conventional stability index for current driven tearing modes [32]. The finite-β term Δ'_β accounts for pressure effects: neoclassical bootstrap drive [43] with finite $\chi_\perp/\chi_{||}$ corrections [44], Pfirsch-Schlüter currents [45] and diamagnetic frequency effects [46]. Pressure effects are indicated here for the sake of completeness only, but we drop them in the following applications where they have negligible influence on the time-scale issue we wish to emphasize in this paper (discussions of Eq. (4) with all the terms retained can be found in references [7,23] which conversely address issues that are critically influenced by pressure effects).

Following the conventional procedure for the calculation of the nonlinear magnetic-island evolution [32], the stabilizing current-drive term writes similarly to the result of reference [22]

$$\Delta'_{CD} = \frac{16\Delta'_{vac}}{ns_s q_a}\frac{I_{CD}}{I_p}\frac{a^2}{\Delta r^2}\frac{1}{\overline{w}^2}\eta_{CD}, \tag{5}$$

where $\Delta'_{vac} = -2m/r_s$ is the *vacuum* Δ', m and n are the poloidal (θ) and toroidal (ϕ) mode number, respectively, s_s is the magnetic shear on the resonant surface $r=r_s$ where $q=m/n$, q_a is the safety factor at the plasma surface r=a, I_p is the total plasma current, I_{CD} is the time-dependent RF-driven current (related to the coupled RF-power through the current-drive efficiency: $\bar{n}_e R_0 I_{CD} = \gamma_{CD} P_{RF}$, where $\bar{n}_e$ is the average electron density and R_0 the tokamak major radius), Δr is the radial width of the RF-driven current channel and $\bar{w} = w/\Delta r$. It is clear from equation (5) that higher RF-power and/or better RF radial-localization lead to improved stabilization. The so-called *stabilization efficiency* η_{CD} is similar to that appearing in reference [22] (where it is noted η_{aux}), but hereafter extends to a more general RF-driven source-term, formally expressed in terms of the current density

$$j_{RF} = j_{RF}^{peak}(t)\, e^{-|2(r-r_0)/\Delta r|^{2\nu}}\, \Pi(\theta_0(t),\Delta\theta)\, \Pi(\phi_0(t),\Delta\phi). \qquad (6)$$

There j_{RF}^{peak} is the time-dependent peak-amplitude at the RF-deposition mean-radius $r=r_0$, and ν is a radial-shape exponent (gaussian [50] for $\nu = 1$, square-box [22] for $\nu \rightarrow +\infty$). The square-box function $\Pi(x_0,\Delta x)$, equal to 1 for $|x-x_0|<\Delta x/2$ and 0 otherwise, defines the time-dependent (θ,ϕ)-domain where the RF-wave interacts with the plasma. It is convenient to introduce

- the helical coordinate $h=m\theta-n\phi-\omega t$, such that (for $n\Delta\phi/m\Delta\theta \ll 1$) the above (θ,ϕ)-domain can be represented in terms of an equivalent h-domain $\Pi(h_0,\Delta h)$, where $h_0=m\theta_0-n\phi_0-\omega t$ and $\Delta h=m\Delta\theta+n\Delta\phi$;

- the normalized perturbed flux-function $\Omega = 8x^2/w^2 - \cos(h)$ [22], where $x=r-r_s$ is the departure to the magnetic surface where the considered mode is resonant;

- the flux-surface-average operator $\{X(\Omega,h)\}_\Omega = \oint dh\, X(\Omega,h)(\Omega+\cos(h))^{-1/2}$ [22], where the h-integration extends from $-h_\Omega$ to h_Ω, with $h_\Omega=\pi$ for $\Omega>1$ (outside island) and $h_\Omega=A\cos(-\Omega)$ for $-1<\Omega<1$ (inside island).

Then, considering the flux-surface average of the parallel projection of the Ohm's law $E_{\|} = \eta(j_{tot}-j_{RF})$, the RF contribution to equation (4) is obtained, as given by equation (5) with

$$\eta_{CD} = \int_{-1}^{+\infty} d\Omega \frac{R(\Omega)}{S(\Omega)} \bar{j}_{RF}(\Omega) \Big/ \int_{-1}^{+\infty} d\Omega \bar{j}_{RF}(\Omega), \tag{7}$$

where both $R(\Omega)=\{\cos(h)\}_\Omega$ and $S(\Omega)=\{1\}_\Omega$ are explicited in terms of elliptic integrals in appendix A, and

$$\bar{j}_{RF}(\Omega) = \left\{\Pi_h \exp(-|\bar{w}(\bar{x}-\bar{x}_0)|^{2\nu})\right\}_\Omega, \tag{8}$$

where $\bar{x} = \left((\Omega+\cos(h))/2\right)^{1/2}$, $\bar{x}_0 = 2(r_0-r_s)/w$. The function Π_h characterizes the (θ,ϕ)-structure (reminiscent of the functions $\Pi(\theta_0(t),\Delta\theta)$ and $\Pi(\phi_0(t),\Delta\phi)$ in equation (6)) of the plasma-wave interaction, which occurs on a finite time-scale τ_c (effective collision time of resonant electrons, of order 1 msec) as discussed in section 2. In reference [50], where it was implicitely assumed that $\omega\tau_c \gg 1$, the function Π_h (M with the notations of [50]) was taken equal to 1 over the h-domain directly affected by the RF-power deposition ($h_0^{on} - \Delta h/2 < h < h_0^{off} + \Delta h/2$, with $h_0^{on/off}$ the value of $h_0(t)$ at the RF switch on/off) and equal to 0 elsewhere. However, as for the ITER parameters emphasized in this paper, the assumption that $\omega\tau_c \gg 1$ is invalid for magnetic islands whose propagation frequency ω is of the order of a few kilo-Hertz or less. A general complex expression is obtained for Π_h, following the procedure discussed in appendix B

$$\Pi_h = \left\{\frac{1-e_{\Delta h}}{1-e_{2\pi}} e_{2\pi-\Delta h} + \left(1-\frac{1-e_{\Delta h}}{1-e_{2\pi}} e_{2\pi-\Delta h}\right)\left(1-e_{h_0+\Delta h/2-h}\right)\right\} \Pi_h^{on},$$

$$\text{for } |h-h_0| < \Delta h/2; \tag{9a}$$

$$\Pi_h = \left\{\frac{1-e_{\Delta h}}{1-e_{2\pi}} e_{2\pi-\Delta h} + \left(1-\frac{1-e_{\Delta h}}{1-e_{2\pi}} e_{2\pi-\Delta h}\right)\left(1-e_{\Delta h}\right)\right\} e_{h_0-\Delta h/2-h}\, \Pi_h^{on},$$

$$\text{for } |h-h_0| > \Delta h/2; \tag{9b}$$

where $e_X = \exp(-X/\omega\tau_c)$, and $\Pi_h^{on}(h) = 1$ for $h_0^{on} - \Delta h/2 < h < h_0^{off} + \Delta h/2$ and 0 otherwise (i.e., no source for island regions which pass by the RF-interaction domain

when the power is off). Then, the stabilization efficiency η_{CD} is a function of the following parameters: the normalized island-width $\bar{w}$, the radial-shape exponent ν, the RF-deposition radial-shift $\bar{x}_0$ with respect to the resonant surface r_s, the angular extent of the RF-interaction Δh, the instantaneous angular location of the RF-interaction $h_0(t)$ and its value $h_0^{on/off}$ at the time of RF switch-on/off, and the island-propagation to plasma-wave-interaction time-scales ratio $\omega\tau_c$. It is useful to introduce the fractional RF-on time $F_{on}=(h_0^{off}-h_0^{on})/2\pi$ (the fraction of time the power is on over a RF-cycle), and the RF-on asymmetry $A_{on}=(h_0^{off}+h_0^{on})/2\pi$ with respect to the O-point (given that the time τ_c for the RF-source ramp is finite with respect to the island transit-time $1/\omega$, some benefit is expected from setting $h_0^{on} < -h_0^{off}$ so that the drive is maximum close to the O-point where h=0). Hence, $\eta_{CD} = \eta_{CD}(\bar{w},\nu,\bar{x}_0,\Delta h,h_0(t),F_{on},A_{on},\omega\tau_c)$ indicates that, in addition to the RF-driven current I_{CD} and its radial-width Δr which appear in equation (5), the RF contribution to the magnetic island evolution is controlled by many parameters, whose influence is discussed in section 6. The dependence of η_{CD} on Δh and $\omega\tau_c$ is illustrated in figure 2.

To conclude this section it is interesting to indicate the way the present results relate with previous references. Reference [22] corresponds to the limit $\bar{J}_{RF}(\Omega) \equiv S(\Omega)$ for $\Omega < \Omega_{CD} = 2/\bar{w}^2 - 1$ and 0 elsewhere (there is no direct link with the function Π_h because the RF source-term j_{RF} is taken as a flux function $j_{RF}(\Omega)$ in [22], so that the radial coordinate $x=r-r_s$ and the helical coordinate $h=m\theta-n\phi-\omega t$ are mixed-up in the flux function Ω rather than treated separately as in the present definition of j_{RF}). Reference [50], with $\nu=1$ and $\bar{x}_0 = 0$, corresponds to the limit where the function Π_h is equal to 1 for $|h| < h_0^{off} = -h_0^{on}$ and 0 elsewhere (i.e., from equation (9), to $\omega\tau_c \rightarrow \infty$ and $\Delta h \rightarrow 0$).

4. WAVE PROPAGATION AND ABSORPTION

From the discussion presented in the previous sections, the basic requirements of a current drive system optimized for tearing mode stabilization are: i) the maximization of the driven current at the island O-point by appropriate toroidal, poloidal and radial localization of the power absorption; ii) the capability to fine tune the launched wave spectrum and/or the wave frequency to track the position of the island in real time during a discharge; iii) the fastest response possible of the current source to power modulation; iv) the ability to drive current off-axis with high efficiency. The first three requirements naturally indicate EC waves as the leading candidate for this function in a reactor. On the other hand, LH waves are favoured by their high CD efficiency, irrespective of the trapped particle fraction. For this reason, calculations will be performed for both types of waves, to make a fair comparison of their merits and drawbacks. In order to describe the wave propagation, ray-tracing codes are appropriate, for both LH [47] and EC [48] waves. In both cases, Fokker-Planck codes are used to compute the self-consistent quasilinear wave damping, which in the case of LH waves can be significantly different from the linear one. Calculations are performed in a standard ITER equilibrium [38], with assumptions of good coupling properties at the plasma edge (which for LH waves is non-trivial) and a launching geometry inspired by the present version of the ITER antennas design [49]. For the electron density and temperature, the following profiles are used

$$n_e(\psi) = (n_{e0} - n_{ea})(1 - \psi^{\beta_n})^{\alpha_n} + n_{ea}$$

$$T_e(\psi) = (T_{e0} - T_{ea})(1 - \psi^{\beta_T})^{\alpha_T} + T_{ea}$$

$$n_{e0} = 1.3 \times 10^{20} m^{-3} \; ; \; n_{ea} = 10^{19} m^{-3} \; ; \; \beta_n = 1 \; ; \; \alpha_n = 0.2$$

$$T_{e0} = 22 \; keV \; ; \; T_{ea} = 1 \; keV \; ; \; \beta_T = 1.85 \; ; \; \alpha_T = 2$$

The m = 2 surface is assumed to be at $\rho_s \approx 0.8$, where $n_e(\rho_s) \approx 1.1 \times 10^{20}$ m^{-3}, $T_e(\rho_s) \approx 7.5$ keV. The other general parameters are: $R_0 = 8.14$ m, a = 2.8 m, elongation $\kappa = 1.6$, $I_p = 21$ MA, $B_0 = 5.7$ T, Z = 1.6, $P_{rf} = 50$ MW.

4.1. LH waves

For reactor-like parameters, LH waves typically cannot penetrate to the plasma core, owing to simultaneous limitations imposed by wave accessibility and Landau damping. Even for a rather peripheral location, such as $\rho_s \approx 0.8$, the propagation window is narrow, because of the extreme flatness of the standard ITER density profile. For density profiles more similar to those measured in present-day tokamaks, such a limitation would be removed. On the other hand, the regime of first-pass absorption, which is essential in order to get poloidally, toroidally and radially localized power deposition [24], is easily obtained. The calculations have been done for a wave frequency of 5 GHz, and a very narrow $n_{||}$ spectrum, which is required to match the power deposition to the narrow propagation window: the injected parallel refractive index spectrum is assumed to be a Gaussian centred at $n_{||} = 2$ and of half-width $\Delta n_{||} \approx 0.1$. Poloidal projections of some rays of $n_{||} = 2$, launched by a coupler located just below the plasma mid-plane, are shown in Fig. 3. The black symbols indicate the beginning and the end of the regions where the wave power is absorbed. Note that the rays do not yet diverge in that region, thus satisfactory poloidal localization inside an m = 2 magnetic island can be achieved. The damping is also localized toroidally, since LH waves roughly follow the field lines. For the three rays of Fig. 3, a toroidal spread of the damping region along a helical magnetic line $\Delta\varphi \approx 40° - 80°$ is found. These figures are compatible with the poloidal and toroidal extensions of an m = 2 magnetic island. The absorbed power density profile and the corresponding driven current, computed by combining ray-tracing and Fokker Planck codes [47] (neglecting for the moment the induced electric field) are shown in Fig. 4. The strong first-pass damping

and the narrowness of the wave spectrum yield a current source radially well localized (full width $\Delta\rho \approx 0.1$). This case corresponds to the total driven current shown in Fig. 1(a), $I_{CD} \approx 1.8$ MA, i.e., 8.6 % of the total plasma current.

4.2. EC waves

In contrast with the case of LH waves, penetration to the core of an ITER-like plasma is not a problem for EC waves in the upshifted frequency regime, namely for $f > f_{ce}$, where f is the wave frequency and f_{ce} is the electron cyclotron frequency. What should be optimized is rather the CD efficiency γ_{CD} for a well localized power deposition, i.e., the parameter $\gamma_{CD}/(\Delta\rho)^2$. Now, the CD efficiency increases with p, where pis an average resonant parallel momentum which, in regimes of strong absorption and for $f > f_{ce}$, is roughly given by $p/m_e c \approx N_{||}(f/f_{ce})$, where $N_{||} < 1$ is the parallel refractive index of the EC waves, and c is the speed of light. This means that the optimum efficiency is obtained for high frequency and high values of the toroidal injection angle with respect to the normal to the magnetic field, $\phi_i = \arcsin(N_{||})$. However, the two parameters $N_{||}$ and f/f_{ce} cannot be independently maximized, being related by the constraint that the power absorption should be located around $\rho \approx \rho_s$. Moreover, for large $N_{||}$, the Doppler broadening of the power absorption profile becomes large, which deteriorates the ratio $\gamma_{CD}/(\Delta\rho)^2$. Since good localization is clearly more important than efficiency, the best compromise cannot be found at extremely large toroidal injection angles. Another free parameter, which can also help in getting the required position of wave damping at optimum values of $N_{||}$ and frequency, is the poloidal injection angle θ_i.

The ITER EC heating and CD system, in the present design status [49], makes use of gyrotrons at f = 170 GHz and with 1 MW unit power. The launching system is an array of 7×8 toroidally steerable mirrors, with fixed θ_i, launching Gaussian beams (2.5 cm waist) horizontally. Ray-tracing calculations based on this system show that

well localized wave absorption at $\rho \approx 0.8$ cannot be achieved. The possibility is then either to design launchers equipped with poloidally steerable mirrors, which introduces a significant technological complication, as discussed in Ref. [50], or to lower the wave frequency. The latter option is considered here. In the geometrical configuration of the present ITER EC launcher, the quantity $\gamma_{CD}/(\Delta\rho)^2$ has a rather broad maximum, as a function of frequency, around f = 140 GHz, which is then assumed as the typical wave frequency. The case of the first harmonic ordinary mode is considered. The constraint of wave absorption at $\rho \approx 0.8$ then imposes, e.g., for the beams launched by the row of antennas in the equatorial plane, $\phi_i = 31°$. If all the beams have to be absorbed at the same flux surfaces, different toroidal injection angles have to be chosen for the 7 horizontal rows of mirrors, in order to compensate for the $N_{||}$ variations due to the orientations of the poloidal field at different vertical elevations. Examples of ray trajectories resulting from such a choice are given in Fig. 5 (a and b, poloidal and toroidal projections, respectively), where only 7 rays are traced, simulating the 7 horizontal rows of injected beams. Each Gaussian beam will have its waist rather close to the launching mirror, then it will be very slightly divergent as it penetrates into the plasma. In this case, multiple ray tracing is adequate to simulate the beam propagation [51], if the typical transversal size of the Gaussian beam is used. The absorbed power density profiles of the 7 beams are shown in Fig. 6. The different power deposition profiles are hardly distinguishable, thus good radial overlapping of the various absorbed powers is achieved, with a total width $\Delta\rho \approx 0.1$, a figure which is not easily improvable. In fact, in this regime the power deposition width is dominated by the beam size, rather than by the Doppler width of the intrinsic absorption line, thus no significant reduction of $\Delta\rho$ can be expected by lowering $N_{||}$. The steady state current density profile (driven by the total 50 MW of EC power), computed by the Fokker-Planck code [37] is shown in Fig. 7. In general, poloidal and toroidal localization of the power deposition inside the island can be optimized by independently phasing in

time the power modulations of the gyrotrons connected with the different horizontal rows of launchers, in order to turn the power of every beam on when the O-point intersects the trajectory of the beam. This requires a very sophisticated imaging system of the 3-dimensional structure of the island in real time, to control the feedback loop.

In conclusion, satisfactory localization of wave absorption can in principle be obtained with both types of waves, with similar values of $\Delta\rho \approx 0.1$. For EC waves, this depends little on the plasma density, whereas for LH waves a relatively narrow window of operation is available, and this window critically depends on the electron density and temperature profiles. Moreover, the toroidal and poloidal localization is expected to be more easily achieved for EC than for LH waves. Conversely, the CD efficiency is about 7 times larger for LH waves.

5. DYNAMIC EFFECTS: NUMERICAL RESULTS

Numerical simulations are now presented, concerning the space and time dependence of the induced electric field, obtained from the simultaneous solution of Eqs. (1)-(3), for the two cases discussed in the previous sections, i.e., 50 MW of LH or of EC waves. The Fokker-Planck code is run on a ($128 \times 128 \times 51$) mesh in the (p, θ_0, ρ) variables, where $\theta_0 = \arccos(p_{\|0}/p)$, and $p_{\|0}$ is the parallel momentum on the equatorial plane at the low field side. The time step is $\Delta t/\tau_e = 0.05$ for LHCD and 0.01 for ECCD. In order to describe the EC quasilinear diffusion coefficient correctly, the wave $N_\|$ spectrum is split into 400 rays, and the damping is evaluated for each of them. In this way, the evolution of the wave beams inside the plasma, as the wave power is absorbed, is accurately evaluated. In this regime (upshifted frequency, high temperature, large trapped electron fraction) it is found that such a large number of rays

is required to obtain stable results. The simulation is first set up by producing an ohmic current density profile, running the Fokker-Planck code without RF power terms. A total plasma current I_p = 21 MA is obtained using a radially constant electric field, corresponding to a loop voltage V_{loop} = 0.068 Volts; the current density profile obtained is shown in Fig. 8. Note that the electrical conductivity calculated by the code corresponds well with standard expressions typical of the banana regime (e.g., [52]), because of the particular form of the collision operator used [42].

The RF power is then turned on. In contrast with the results of Fig. 1, obtained without an electric field, the total current and also the current density profile now remain constant, except for some weak transient oscillations which would be barely visible on the scale of Fig. 8. On the other hand, a large hole in the parallel electric field profile, initially constant, appears, in the region where the waves are absorbed. This is shown in Fig. 9 for LH waves, and in Fig. 10 for EC waves. In both figures, the rise phase of the back emf is presented, at a sequence of equally spaced times, until the induced electric field attains a short-time-scale stationary value. This is the relevant phase in order to describe each modulation correctly. Note that, in the case of ECCD, the evolution starts with an increase of $E_{||}$, due to the phenomenon of the Ohkawa current.

Then, the full modulation phase is computed. For an ITER plasma, the island rotation frequency is expected to be of the order of the diamagnetic frequency in ohmic plasmas, i.e., 0.1 - 0.2 kHz, and much higher (of the order of a few kHz) in Neutral-Beam heated discharges. The computed electric field at ρ = 0.8, during a few modulation cycles at f_{mod} = 0.2 kHz, is shown in Figs. 11 and 12, for LHCD and ECCD, respectively. The square modulation patterns are also shown, at the bottom of the two figures. In the case of LHCD, $E_{||}$ does not completely attain its stationary value at the end of the power pulse, and the full no-power time interval is necessary to marginally recover its value in the ohmic phase. A reduction of the stabilization

efficiency can be anticipated in connection with this behaviour. ECCD is characterized by a faster, but more complex response: at the beginning and at the end of each power pulse, a large, opposite $E_{||}$ variation takes place, lasting for 200 μs approximately, due to the Ohkawa current. As the modulation frequency increases, the excursions of $E_{||}$ around an average value become smaller and smaller. This is shown in Fig. 13, in the case of LH waves, for three different modulation frequencies, i.e., f_{mod} = 0.2, 1 and 5 kHz. ECCD results are qualitatively similar. Figure 13 illustrates an important effect associated with the transient nature of the modulated current drive phenomenon. If $f_{mod} > \tau_c^{-1}$, the stabilizing perturbation δJ would not attain its maximum value for a given wave power during the heating pulse. Thus, for high island rotation frequency, it is not possible to profit of the available power completely, in order to drive an as large as possible δJ at the island O-point. This implies that the stabilization efficiency can be reduced by the finite time response of the driven current source. Since the modulation frequency is connected with the island rotation frequency, and the current response is intrinsically related to the resonant electron collision rate, this difficulty cannot be easily removed.

6. ISLAND WIDTH EVOLUTION

The island width evolution equation (Eq. 4) is now solved, evaluating the perturbation δJ with the computed induced electric field and describing the angular dependence of the current source term by means of the previously discussed square-box model. Neoclassical effects are neglected, and the case of a positive Δ' tearing mode is considered. Values of $\Delta' = (10/a)(1 - w/w_s)$ and $s_s = 1$ are considered, where w_s is the saturated island width (here, $w_s/a = 0.2$ is used). The current perturbation is

assumed to be exactly centred at the resonant surface (i.e., at $\rho = \rho_s$), and modifications of the equilibrium q-profile are neglected. The island width evolution for 50 MW of LHCD is shown in Fig. 14. First, note that the time scale for significant reduction of the island width is lower than τ_ρ ($\approx$ 50 s in this case). Thus, the assumption of an essentially unperturbed current profile is satisfied. In all the cases presented here, complete stabilization of the m = 2 mode is eventually achieved; however, the model considered here is not strictly applicable to the vanishing island width limit, in which transverse diffusion has the effect of removing the divergence of η_{CD}. This delicate limit is discussed in Appendix C. The dashed curve represents the ideal limit, in which the wave power stays centred at the island O-point: it is obtained by neglecting island rotation effects (h_0 = constant). If the island is allowed to rotate at the frequency f_{mod}, the stabilization becomes slower, as shown by the two solid curves. The frequency dependence of the island width evolution reflects the complicated behaviour of the function $\eta_{CD}(\omega\tau_c)$, discussed in Sec. 3.

The effect of modulating the wave power is illustrated in Fig. 15, for f_{mod} = 5 kHz. The dashed curve represents the non-modulated case (F_{on} = 1), in which the value of Δh is immaterial, whereas the case of 50 % duty cycle modulations (F_{on} = 0.5) is illustrated by the solid curves, for two different values of Δh. It appears that modulating the wave power is advantageous only if the current source is well concentrated poloidally and toroidally, which is generally the case for ECCD, but not necessarily for LHCD. The fact that stabilization is achieved for a uniform distribution of the current over the island (including the O-point, but the X-point as well) is related to the peculiar structure of the $R(\Omega)$ function, discussed in Appendix 1. In the case of an angularly broad power deposition, the larger current associated to a steady power input more than compensates for the destabilizing contribution related to the X-point.

Critical parameters for the stabilization efficiency are the values of the current perturbation width $\Delta\rho$ and of the shift between the radial position ρ_0 of the maximum

δJ and that of the resonant surface ρ_s. As illustrated by Fig. 16 and in view of the $1/(\Delta\rho)^2$ dependence of the stabilizing term, an increase of $\Delta\rho$ has a strong negative impact on the stabilization efficiency. The shift $\rho_s - \rho_0$ has a similar effect. This implies that an accurate feedback should be implemented, not only to phase the power modulations with the O-point position, but also to keep the maximum power deposition as close as possible to the resonant surface.

Finally, a comparison between ECCD and LHCD for the same wave power, F_{on} = 0.5 and f_{mod} = 0.2 kHz is shown in Fig. 17, assuming the same radial power deposition width. Despite the advantage related to the better angular localization of the ECCD ($\Delta h \approx \pi/10$ with respect to $2\pi/3$ for LHCD), the time required for a full stabilization of the mode is much longer, because of the large difference in the CD efficiency. This suggests the possibility of using LHCD at a lower power level, in order to attain full stabilization in a time of the order of 30 to 40 s.

7. DISCUSSION AND CONCLUSIONS

On the basis of the results presented in the previous sections, the potential of using RF current drive for tearing mode stabilization in a tokamak reactor can be discussed. This is a complex problem, involving several physical effects, such as wave propagation and absorption, kinetic response of the electron velocity distribution, MHD phenomena, as well as time scales varying over five orders of magnitude. Although the analysis presented in this paper is by no means complete, an attempt has been made to combine several of the most relevant physical effects into a dynamic model, in particular focusing on the role of time-dependent effects. It has been shown that such effects are both conceptually and quantitatively important, and should

generally be included in the analysis of the problem. Several important points, in part already appearing in the literature, but not generally recognized, can be summarized as follows:

i) Fast modulations (of the order of the kHz) of RF driven currents are impossible, being limited by both kinetic and inductance effects. However, modulations of the back emf provides an equivalent stabilizing effect.

ii) The critical parameter defining the stabilization efficiency is $\gamma_{CD}/(I_p(\Delta\rho)^2)$. The radial shift of the non-inductive current maximum with respect to the resonant surface also plays an important role, substantially equivalent to that of $\Delta\rho$.

iii) The time necessary for a significant reduction of the island size depends on the island rotation frequency. The advantage of modulating the wave power is limited and generally depends on the angular extent of the power deposition.

iv) As far as the comparison between LHCD and ECCD is concerned, a clear advantage in using LHCD (a factor of 7 in the CD efficiency), at least for ITER parameters, exists.

In fact, in a large machine, a power deposition width of $\Delta\rho \approx 0.1$ appears marginally achievable for LHCD, and this is also a reasonable lower limit for ECCD. On the basis of simple considerations of propagation and absorption properties, lower values of $\Delta\rho$ seem unrealistic for both CD methods. Radial diffusion effects can be quantified by using the same kinetic model [24] and are likely to moderately increase this value. Although in principle LHCD appears a more suitable method, its use in a reactor for this function is subject to many more uncertainties than ECCD. The main problem is that first-pass absorption in the region $\rho \approx \rho_s$ is critically dependent on the density and temperature profiles and the useful window is rather narrow for very flat density profiles. Moreover, a very narrow $n_{||}$ spectrum is required and must be accurately controlled, in order to centre the power deposition on the resonant surface with a good precision. These requirements are probably more easily satisfied by an

ECCD system specifically dedicated to this task. In addition, the power deposition profile of EC waves is virtually independent of the density profile and the time response of ECCD, in the case of a modulated power input, is faster by a factor of 4-5.

Assuming that a reasonable compromise is found between the various advantages and drawbacks of the two systems, the final choice for ITER should result in a system capable of substantially reducing the island width in a time of the order of 30 s, by use of 30-50 MW of unmodulated power. Then, the question is whether this would be adequate for a reactor. To prevent a disruption [7], the island width should nominally satisfy the condition $w/a < (1-\rho_s)$, thus reducing the island size to a value $w/a \approx 0.1$ appears sufficient. As far as reduction in confinement is concerned, simple estimates of the global effect of the presence of an island of this size [52] yield a reduction of the energy confinement time of the order of 20 %, which could be tolerable. If a complete elimination of the islands would turn out to be impossible because of saturation effects not included in the present model, then a significant fraction of the total additional heating power of ITER should be steadily applied to this task. Indeed, a large power ($\geq$ 100 MW) is expected to be necessary in the early phase of the discharge, to enter the H mode during the density ramp, and such a power would be available in the following burn phase. What should be developed is a control strategy combining RF current drive inside the islands, as a relatively fast method of reacting to the appearance of unstable profiles, with other means of constraining the evolution of the discharge towards a state in which tearing modes are stable.

Acknowledgements

Useful discussions with F. Perkins, T. Hender and H. Zohm are gratefully acknowledged. This work was partially supported by USDOE under Contract AC02-76-CH0-3073.

Appendix A: Functions R(Ω) and S(Ω)

In section 3, we have introduced the flux-surface-average operator $\{X(\Omega,h)\}_\Omega$ and the functions $R(\Omega)=\{\cos(h)\}_\Omega$ and $S(\Omega)=\{1\}_\Omega$. The latter play an important role in the calculation of the magnetic island evolution, which makes it worth giving some of their characteristics.

$$\left.\begin{aligned} S(\Omega) &= \frac{\sqrt{2}}{\pi}K(m) \\ R(\Omega) &= \frac{\sqrt{2}}{\pi}(2E(m)-K(m)) \end{aligned}\right\} \text{ for } -1 \le \Omega \le 1 \text{ (inside island)}, \qquad \text{(A1.a)}$$

$$\left.\begin{aligned} S(\Omega) &= \frac{\sqrt{2}}{\pi}\frac{K(1/m)}{\sqrt{m}} \\ R(\Omega) &= \frac{\sqrt{2}}{\pi}\frac{2mE(1/m)-(2m-1)K(1/m)}{\sqrt{m}} \end{aligned}\right\} \text{ for } \Omega \ge 1 \text{ (outside island)}, \qquad \text{(A1.b)}$$

where $m=(\Omega+1)/2$ and K and E are the complete elliptic integrals

$$\left.\begin{aligned} K(m) &= \int_0^{\pi/2} d\alpha\,(1-m\sin^2\alpha)^{-1/2} \\ E(m) &= \int_0^{\pi/2} d\alpha\,(1-m\sin^2\alpha)^{1/2} \end{aligned}\right\} \qquad \text{(A2)}$$

The profiles of the functions R(Ω) and S(Ω) are illustrated in figure A1. It is important to note that R(Ω) and S(Ω) asymptotically ($\Omega\to\infty$) behave like $\Omega^{-3/2}$ and $\Omega^{-1/2}$, respectively. Also, the fact that R(Ω) changes sign for $\Omega=\Omega_0\approx 0.64$, while S(Ω) is strictly positive, relates to the property that a RF-driven current with the appropriate sign ($\mathbf{j_{RF}}.\mathbf{B_{eq}}>0$ for $s_s>0$) is stabilizing when located in the vicinity of the island O-point ($\Omega<\Omega_0$) while it is destabilizing outside the region limited by the flux surface $\Omega=\Omega_0$ lying in between the O-point ($\Omega=-1$) and the separatrix ($\Omega=1$). Finally, a key property, in the context of the validity of the asymptotic matching procedure discussed in appendix C for $w<\Delta r$, is that

$$\int_{-1}^{+\infty} d\Omega\, R(\Omega) = 0. \qquad \text{(A3)}$$

Appendix B: Calculation of the function Π_h for finite $\omega\tau_c$.

As mentioned in section 3, reference [50] implicitely considers the limit $\omega\tau_c \to \infty$ and $\Delta h \to 0$. The present paper thus appears as a generalization of the latter work, in a way that is clarified in this appendix.

From equation (6), one would expect that $\Pi_h = \Pi(h_0(t),\Delta h)$ (at least for the *reasonable* limit $n\Delta\phi/m\Delta\theta \ll 1$, so that actual trapeze-box resulting from the product of the Π square-box functions for θ and ϕ leads to a square-box for h). However, this would not take the finiteness of the RF time-scale τ_c into account. The latter implies that the resonant electrons keep carrying some of the momentum they have acquired (during their transient interaction with the RF-wave) after they leave the RF interaction region (with the propagating magnetic island they are entrained with): the momentum (i.e., the *effective* current) carried by the resonant electrons exponentially decays with the characteristic time τ_c (see section 2).

In order to model the motion of the magnetic island relative to the RF-interaction region, we consider a propagating square-box for h, $\Pi(h_0(t),\Delta h)$, instantaneously centered at $h=h_0(t)=h_0(0)-\omega t$, and bounded at $h^{\pm}=h_0\pm\Delta h/2$, where Δh is the box-width (see figure B1). At h^+, where the RF-interaction is about to start (for a time $\Delta h/\omega$), there is an *incompletely relaxed* current j_{RF}^0 left from the previous transit of the island. As one moves backwards, for $h^-<h<h^+$, the RF-driven current associated with the considered transit (cycle) of the magnetic island adds to the *incompletely relaxed* current j_{RF}^0

$$j_{RF}(h) = j_{RF}^0 + \left(j_{RF}^{max}(P_{RF}) - j_{RF}^0\right)\left(1 - e^{-(h^+-h)/\omega\tau_c}\right), \qquad \text{(B1)}$$

where $j_{RF}^{max}(P_{RF})$ is the current density driven with an RF-power P_{RF} in steady state. As one moves further backwards, for $h^+-2\pi<h<h^-$, the *incompletely relaxed* current left from the considered transit of the magnetic island is

$$j_{RF}(h) = j_{RF}^- e^{-(h^- - h)/\omega\tau_c}, \qquad \text{(B2)}$$

where

$$\bar{j}_{RF} = j_{RF}(h^-) = j_{RF}^0 + \left(j_{RF}^{max}(P_{RF}) - j_{RF}^0\right)\left(1 - e^{-\Delta h/\omega\tau_c}\right). \quad \text{(B3)}$$

Then, considering that the magnetic island imposes a periodicity constraint on h: $h \equiv h + 2\pi$, one finds an expression relating j_{RF}^0 to $j_{RF}^{max}(P_{RF})$

$$j_{RF}^0 = j_{RF}^{max}(P_{RF}) \frac{1 - e^{-\Delta h/\omega\tau_c}}{1 - e^{-2/\omega\tau_c}} e^{-(2\pi - \Delta h)/\omega\tau_c}. \quad \text{(B4)}$$

This allows to express the function Π_h as given by equation (9), where the *filter* Π_h^{on} accounts for the existence of an h-domain where no RF power is applied (modulated RF power, with fractional on time F_{on}). The structure of the function Π_h is illustrated in figure B2 for various values of the island-propagation to plasma-wave-interaction time-scales ratio $\omega\tau_c$.

The function Π_h, as defined in equation (9), is normalized in order to exclusively reflect the spatial structure of the plasma-wave interaction, through the stabilization efficiency η_{CD} in equation (5), while the strength of the interaction is characterized by the RF-driven current I_{CD}, which is assumed proportional to the RF-power P_{RF}, with the constant current-drive efficiency γ_{CD}: $\bar{n}_e R_0 I_{CD} = \gamma_{CD} P_{RF}$. This procedure amounts to normalizing the amplitude of the RF source-term j_{RF}^{peak} in equation (6) to the total RF-driven current I_{CD} through

$$I_{CD} = 2r_s \int_0^{+\infty} dx \int_0^{2\pi} dh\, j_{RF}^{peak}\, \Pi_h\, e^{-|2(r-r_0)/\Delta r|^{2\nu}} = \frac{\pi r_s \Delta r}{2\sqrt{2}} \overline{w}\, j_{RF}^{peak} \int_{-1}^{+\infty} d\Omega\, \bar{J}_{RF}(\Omega), \quad \text{(B5)}$$

where $\bar{J}_{RF}(\Omega)$ is defined by equation (8). In this respect, the present calculation differs from previous references (except [22]) where there is no magnetic island effect on the relationship between j_{RF}^{peak} and I_{CD}. The dependence of Δ'_{CD} as $1/\overline{w}^2$, as opposed to the *conventional* dependence as $1/\overline{w}$, originates from equation (B5) which is nonetheless obviously ill-defined for a vanishingly small island width $\overline{w} \to 0$.

Appendix C: Small island limit and RF modulations.

We consider an expansion of the exponential appearing in the definition of $\bar{J}_{RF}(\Omega)$ in equation (8):

$$\exp\left(-|\overline{w}(\bar{x}-\bar{x}_0)|^{2\nu}\right)=\sum_{n=0}^{+\infty}\overline{w}^{2n\nu}f_n(\Omega,h), \tag{C1}$$

where

$$f_n(\Omega,h)=\frac{(-1)^n|\bar{x}(\Omega,h)-\bar{x}_0|^{2n\nu}}{n!} \tag{C2}$$

equals 1 for n=0. Then,

$$\eta_{CD}\propto\sum_{n=0}^{+\infty}\overline{w}^{2n\nu}N_n\,, \tag{C3}$$

where

$$N_n=\int_{-1}^{+\infty}d\Omega\frac{R(\Omega)}{S(\Omega)}\{\Pi_h f_n\}_\Omega \tag{C4}$$

At lowest order in the development of η_{CD} with respect to $\overline{w}^{2\nu}$, the zeroth order element is proportional to N_0 and Δ'_{CD} behaves singularly like $1/\overline{w}^2$. As a result of the asymptotic matching (extension of the radial integration domain up to infinity), this term cancels for $\Pi_h=1$ (i.e., $F_{on}=1$ and $\omega\tau_c\to\infty$), since $\{1\}_\Omega=S(\Omega)$ and $\int_{-1}^{+\infty}d\Omega R(\Omega)=0$ (see appendix A). The next-order correction then corresponds to terms of order $\overline{w}^{2\nu}$ and Δ'_{CD} behaves like $\overline{w}^{2(\nu-1)}$. These exactly compensate the $1/\overline{w}^2$ singularity in Δ'_{CD} (thus leading to a finite Δ'_{CD} for $\overline{w}=0$.) for the critical radial-shape exponent ν=1.

The limit Π_h=1 corresponds to the case when $\omega\tau_c$»1 and there is no modulation on the RF power. It is interesting to consider what the effect of modulating the RF power will be on the above result. To this end, we consider equation (9), where Π_h appears as the product of a shape-function (the curly bracket, associated with finite-$\omega\tau_c$) $F(h-h_0)$ and a modulation-function $\Pi_h^{on}(h)$, which we Fourier decompose to obtain three types of terms:

$$\Pi_h\equiv\sum_{k,k'}\left\{T^e_k+T^e_{k\neq k'}\cos((k-k')h)+T^o_{k\neq k'}\sin((k-k')h)\right\}\cos(k\omega t). \tag{C5}$$

The last type ($T^{o}_{k\neq k'}$) corresponds to h-odd terms which average-out through application of the flux-surface-average operator $\{\ \}_{\Omega}$. The first type (T^{e}_{k}) contributes no term to $\bar{J}_{RF}(\Omega)$: N_0 cancels by application of the flux-surface-average operator $\{\ \}_{\Omega}$ which produces a term proportional to $S(\Omega)$. Then, the only type which contributes a term to the above mentioned Δ'_{CD} singularity (through N_0) is the second one ($T^{e}_{k\neq k'}$). The weight of the latter type of terms, and thus the possibility to benefit from an increasingly strong stabilization at smaller island width, is shown to become all the less significant that $\omega\tau_c$ is larger and that the RF power is less modulated (F_{on} close to 1). Of course, there is a limit to how much one can benefit from the Δ'_{CD} singularity. Indeed, a critical island-width w_{CD} is expected to exist below which the singular behavior of Δ'_{CD} is attenuated, similarly to what happens for the neoclassical drive [44], for instance . The existence of such a critical island-width, induced by diffusion, is analyzed numerically and discussed in a subsequent paper [54].

References

[1] CHANG, Z., et al., Phys. Rev. Lett. **74** (1995) 4663.

[2] ZOHM, H., et al., Plasma Phys. Contr. Fusion **37** (1995) A313.

[3] LA HAYE, R.J., et al., Nucl. Fusion **37** (1997) 397.

[4] ZOHM, H., et al., Plasma Phys. Contr. Fusion **39** (1997) B237.

[5] GATES, D.A., et al., Nucl. Fusion **37** (1997) 1593.

[6] CHANG, Z., et al., Nucl. Fusion **34** (1994) 1309.

[7] SAUTER, O., et al., Phys. Plasmas **4** (1997) 1654.

[8] TROYON, F., et al., Plasma Phys. Contr. Fusion **26** (1984) 209.

[9] HOLMES, J.A., et al., Nucl. Fusion **19** (1979) 1333.

[10] CHAN, V., et al., Nucl. Fusion **22** (1982) 272.

[11] REIMAN, A.H., Phys. Fluids **26** (1983) 1338.

[12] YOSHIOKA, Y., et al., Nucl. Fusion **24** (1984) 565.

[13] RUTHERFORD, P.H., in *Basic Phys. Processes of Tor. Fus. Plasmas* (Proc. Course and Workshop, Varenna, 1985), Vol. 2, CEC, Brussels (1986) 531.

[14] IGNAT, D.W., et al., in *Applications of RF Waves to Tokamak Plasmas* (Proc. Course and Workshop, Villa Monastero, 1985), Vol. 2, CEC, Brussels (1985) 525.

[15] DE LUCA, F., et al., Phys. Fluids **29** (1986) 501.

[16] O'BRIEN, M.R., et al., in *Controlled Fusion and Plasma Heating* (EPS, Geneva, 1986), **10C** II, 270.

[17] WESTERHOF, E., Nucl. Fusion **27** (1987) 1929, and **30** (1990) 1143.

[18] MORRIS, A.W., et al., *1992 Int. Conf. on Plasma Physics,* Innsbruck 1992, (EPS Geneva) vol. 16C part I p. 423.

[19] COX, M., in *Radiofrequency Heating and Current Drive of Fusion Devices* (Proc. of Europhysics Topical Conference 1992), EPS, Geneva, Vol. 16E, p. 37.

[20] KURITA, G., et al., Nucl. Fusion **34** (1994) 1497.

[21] LAZZARO, E., RAMPONI, G., Phys. Plasmas **3** (1996) 978.

[22] HEGNA, C.C., CALLEN, J.D., Phys. Plasmas **4** (1997) 2940.

[23] ZOHM, H., Phys. Plasmas **4** (1997) 3433.

[24] BERNABEI, S., et al., Nucl. Fusion **38** (1998) 87.

[25] HOSHINO, K., et al., Phys. Rev. Lett. **69** (1992) 2208.

[26] SING, D., et al., Phys. Fluids **B5** (1993) 3239.

[27] KISLOV, D.A., et al., Nucl. Fusion **37** (1997) 339.

[28] CAROLAN, P.G., et al., in *21st EPS Conference on Controlled Fusion and Plasma Physics* (EPS, Geneva, 1994), **18B** I, 214.

[29] HOSHINO, K., et al., AIP Conf. Proc. **289** (1994) 149.

[30] McARDLE, G.J., et al., in *Proceedings of the EC-9 Workshop* (World Scientific, Singapore, 1995), 271.
[31] FISCH, N.J., Rev. Mod. Phys. **59** (1987) 175.
[32] RUTHERFORD, P.H., Phys. Fluids **16** (1973) 1903.
[33] GIANAKON, T.A., et al., Phys. Plasmas **3** (1996) 4637.
[34] GIRUZZI, G., Nucl. Fusion **27** (1987) 1934.
[35] OHKAWA, T., *Steady State Operation of Tokamaks by RF Heating*, Report GA-A138476, General Atomics, San Diego, CA, USA (1976).
[36] FISCH, N.J., BOOZER, A.H., Phys. Rev. Lett. **45** (1980) 720.
[37] GIRUZZI, G., Plasma Phys. Contr. Fusion **A35** (1993) 123.
[38] ITER-JCT and Home Teams, Plasma Phys. Contr. Fusion **37** (1995) A19.
[39] ROMANELLI, F., et al., Phys. Fluids B**1** (1989) 1659.
[40] T.A. GIANAKON, et al., International Sherwood Fusion Theory Conference, Madison, April 28-30, 1997, paper 1D13.
[41] KILLEEN, J., et al., *Computational methods for kinetic models of magnetically confined plasmas* (Springer Verlag, New York, 1986).
[42] GIRUZZI, G., et al., Nucl. Fusion **32** (1992) 1011.
[43] QU, W.X., CALLEN, J.D., *Nonlinear Growth of a Single Neoclassical MHD Tearing Mode in a Plasma*, Rep. UWPR-85-5, Univ. of Wisconsin, Madison (1985); CARRERA, R., et al., Phys. Fluids **29** (1986) 899.
[44] FITZPATRICK, R., Phys. Plasmas **2** (1995) 825.
[45] GLASSER, A.H., et al., Phys. Fluids **12** (1975) 875; KOTSCHENREUTHER, M., et al., Phys. Fluids **28** (1985) 294.
[46] SMOLYAKOV, A.I., Plasma Phys. Contr. Fusion **35** (1993) 657; WILSON, H.R., et al., Phys. Plasmas **3** (1996) 248.
[47] CARDINALI, A., in *Proc. of the Joint Varenna-Lausanne Int. Workshop on Theory of Fusion Plasmas*, (E. Sindoni, F. Troyon, J. Vaclavik editors, Varenna 1994), p. 417.
[48] KRIVENSKI, V., et al., Nucl. Fusion **25** (1985) 127.
[49] BOSIA, G., et al., in *Fusion Energy 1996* (IAEA, Vienna, 1997) **2**, 917.
[50] PERKINS, F.W., et al., in *Controlled Fusion and Plasma Physics* (EPS, Geneva, 1997), **21A** III, 1017.
[51] NOWAK, S., OREFICE, A., Phys. Plasmas **1** (1994) 1242.
[52] COPPI, B., SIGMAR, D.J., Phys. Fluids **16** (1973) 1174.
[53] CHANG, Z., CALLEN, J.D., Nucl. Fusion **30** (1990) 219.
[54] GIANAKON, T.A., et al., Phys. Plasmas, to be submitted.

Figure Captions

Fig. 1 Time dependent non-inductive current, evaluated neglecting inductance effects, for the parameters appropriate to stabilization of an m = 2 mode in ITER. The absorbed RF power is 50 MW; the current is driven around $\rho \approx 0.8$.

a) LHCD; b) ECCD.

Fig. 2 η_{CD} vs $\omega\tau_c$ for two different values of Δh.

Fig. 3 Poloidal projections of LH wave trajectories, for three different ray launching positions, and a launched $n_{||} = 2$. The black symbols (squares, dots and triangles, respectively, for the rays starting at θ = -20°, -10°, and 0°) indicate the beginning and the end of the regions where the rays are absorbed.

Fig. 4 Computed absorbed LH power density for an injected spectrum peaked at $n_{||} = 2$ and with half-width $\Delta n_{||} = 0.1$ (right scale); corresponding driven current density (left scale).

Fig. 5 Computed ray trajectories for EC waves at f = 140 GHz, launched horizontally by 7 different poloidal positions, simulating the 7 horizontal rows of mirrors of the ITER launcher. ϕ_i = 24.5°, 27.5°, 29.5°, 31°, 32°, 32°, 32.5°, from top to bottom. For sake of clarity, the rays are not traced completely (anyway, they are absorbed around $\rho \approx 0.8$, on the low field side).

a) poloidal projections; b) toroidal projections.

Fig. 6 Absorbed power density profiles for the 7 beams whose central rays are shown in Fig. 5. The total injected power of 50 MW is evenly distributed on the 7 beams.

Fig. 7 Computed current density profile, for 50 MW of ECCD, corresponding to the power absorption profiles of Fig. 6.

Fig. 8 Computed Ohmic current density profile, for $V_{loop} = 0.068$ Volts.

Fig. 9 Computed electric field profile, for a sequence of evenly spaced times from t = 0 (the RF switch-on time) to t = 2.6 ms, in the case of LHCD.

Fig. 10 As in Fig. 9, for $0 < t < 1$ ms, in the case of ECCD.

Fig. 11 Computed electric field at $\rho = 0.8$ versus time, for an RF power modulated at $f_{mod} = 0.2$ kHz, in the case of LHCD. At the bottom, the square modulation pattern is shown.

Fig. 12 As in Fig. 11, in the case of ECCD.

Fig. 13 As in Fig. 11, for three different modulation frequencies.

Fig. 14 Time evolution of the normalized island width during LHCD, for the parameters of Fig. 11, and an m = 2 tearing mode with $a\Delta' = 10 > 0$. Ideal case with no island rotation effects (dashed line); two cases with LH power modulated at $f_{mod} = 0.2$ kHz and 5 kHz, respectively (solid lines).

Fig. 15 As in Fig. 14, for the case $f_{mod} = 5$ kHz, $F_{on} = 0.5$ (solid lines, for two different values of Δh) and $F_{on} = 1$, i.e., no modulation of the RF power (dashed line).

Fig. 16 As in Fig. 14, for the case $f_{mod} = 0.2$ kHz, and different values of $\Delta\rho$, $\rho_s - \rho_0$.

Fig. 17 Time evolution of the normalized island width during LHCD and ECCD, for the same wave power (50 MW) and $f_{mod} = 0.2$ kHz.

Fig. A1 Functions $R(\Omega)$ and $S(\Omega)$.

Fig. B1 RF-interaction scheme.

Fig. B2 Various examples of the function Π_h, for $F_{on}=1/2$, $A_{on}=0$, $h_0=0$ and $\Delta h=\pi/4$: $\omega\tau_c \ll 1$ (dashed line), $\omega\tau_c=1$ (continuous line) and the case of reference [50] $\omega\tau_c \gg 1$ (dash-dotted line).

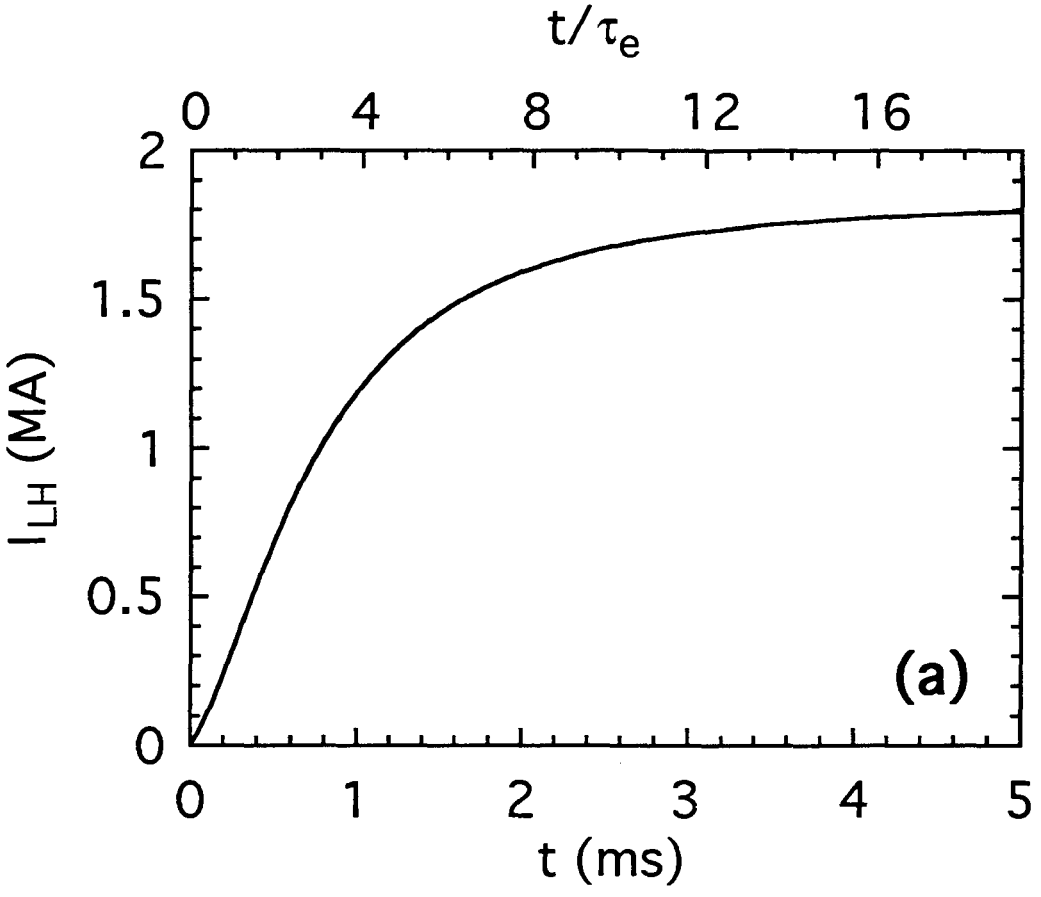

Fig. 1(a)

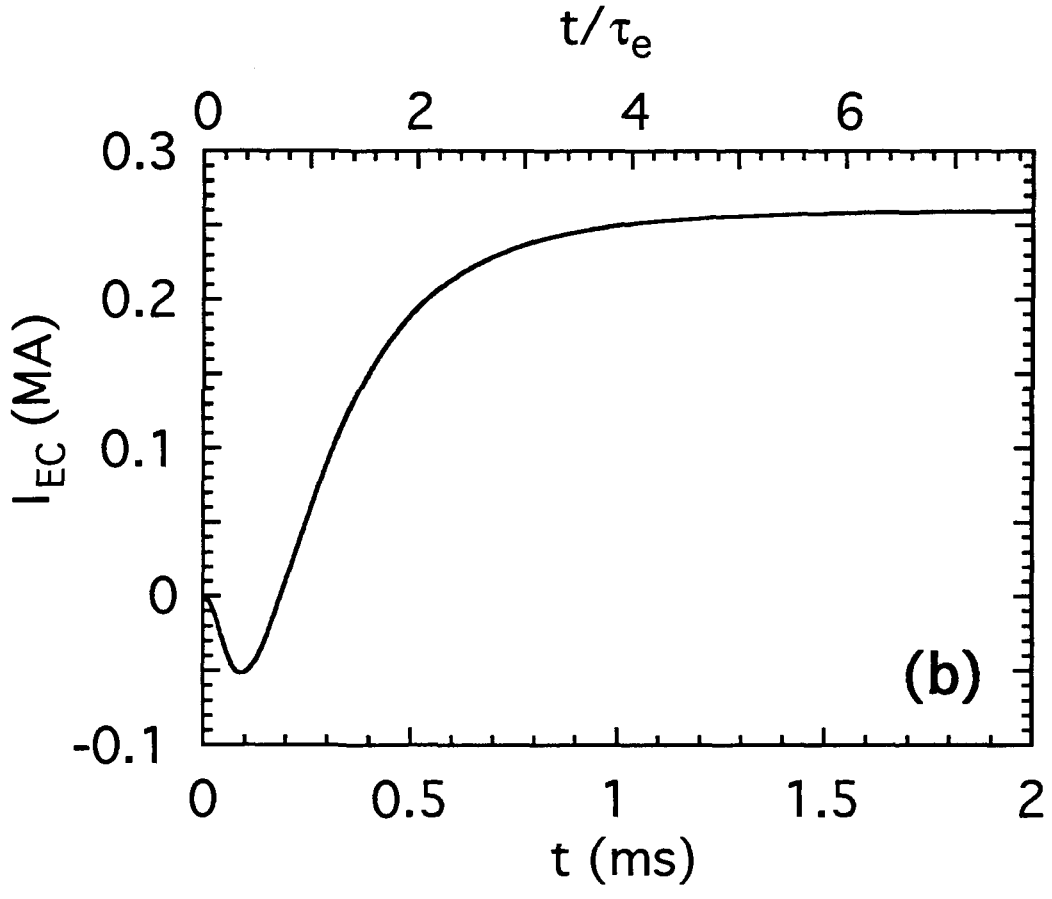

Fig. 1(b)

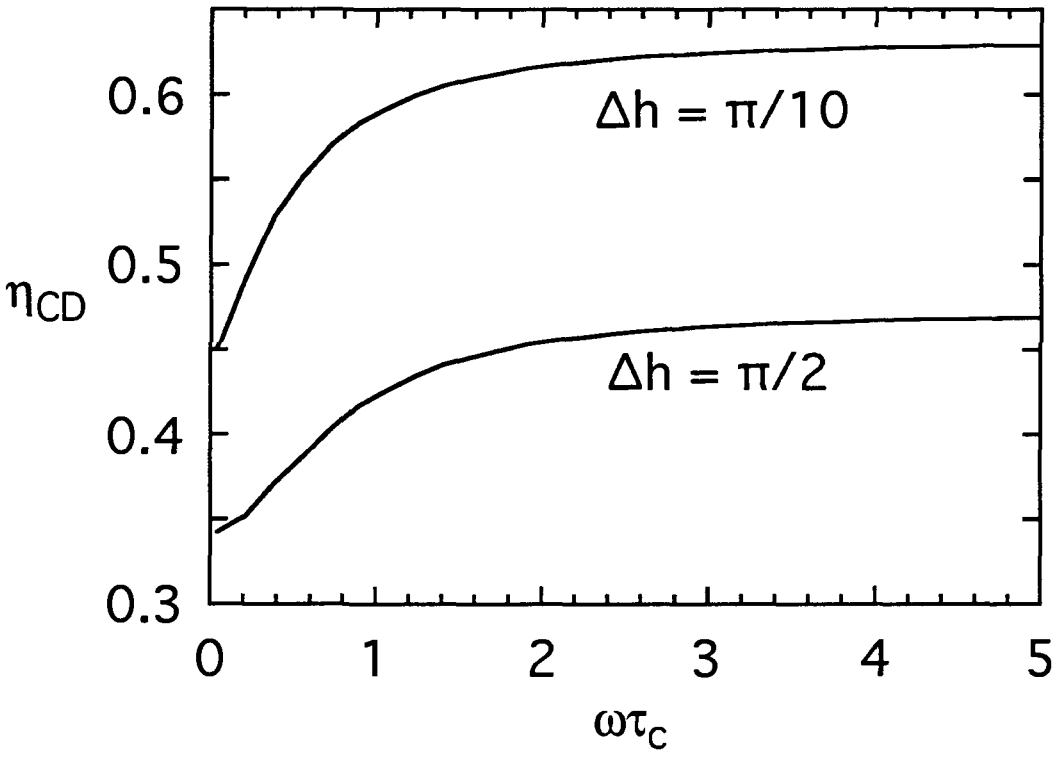

Fig. 2

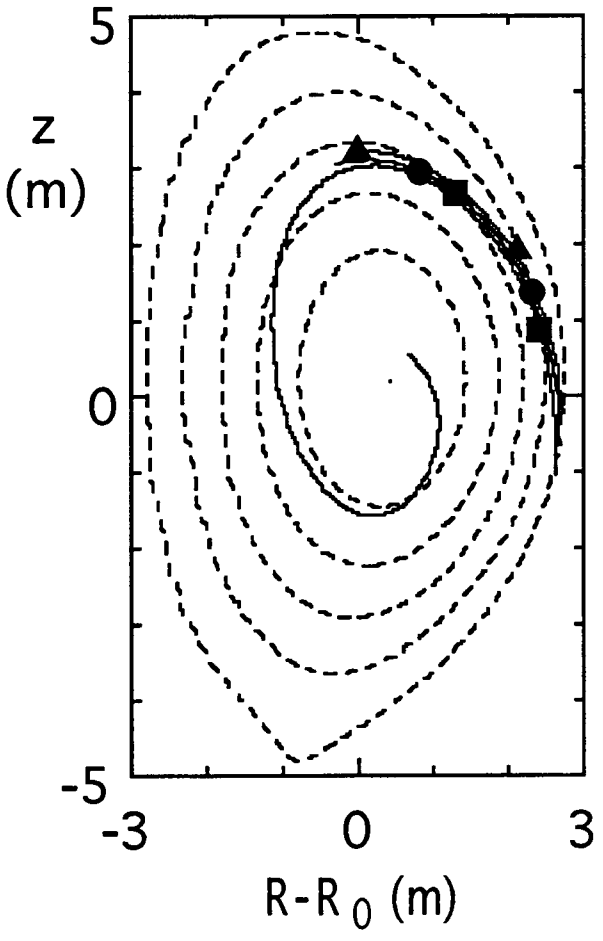

Fig. 3

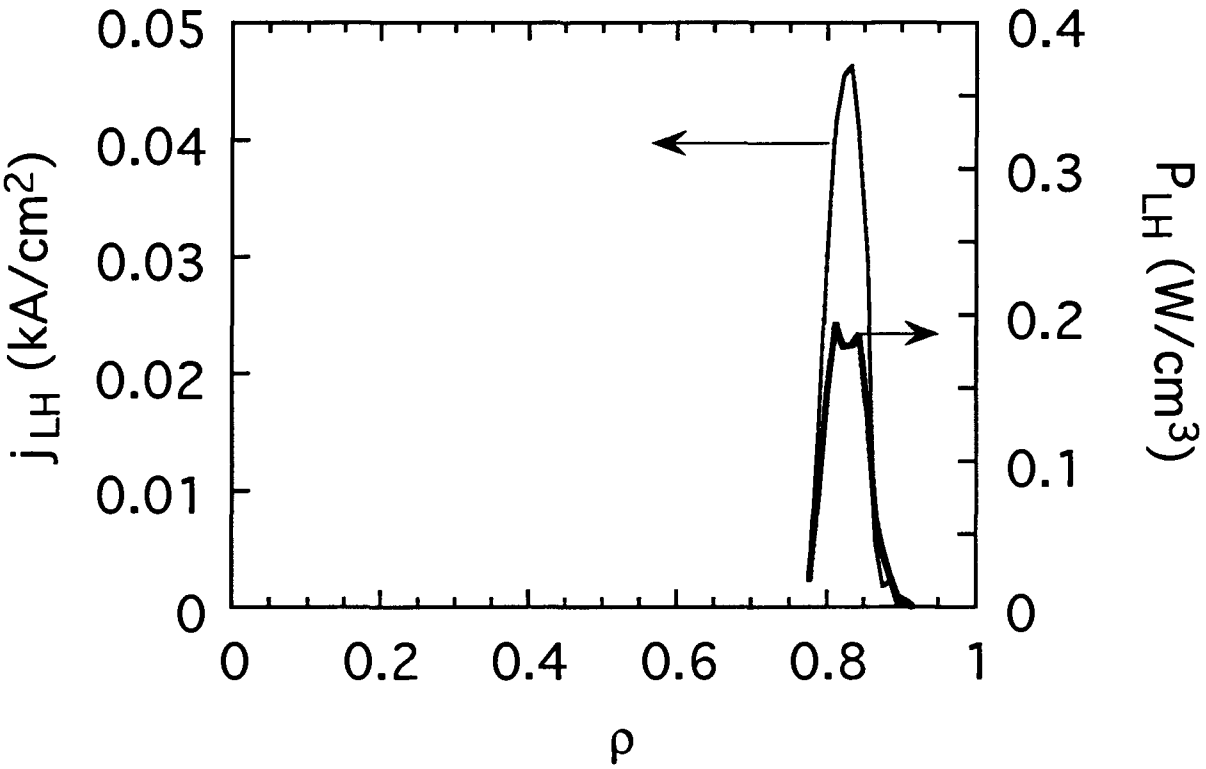
0.05
0.04
0.03
0.02
0.01
0
j_{LH} (kA/cm^2)
0.4
0.3
0.2
0.1
0
P_{LH} (W/cm^3)
0
0.2
0.4
0.6
0.8
1
ρ

Fig. 4

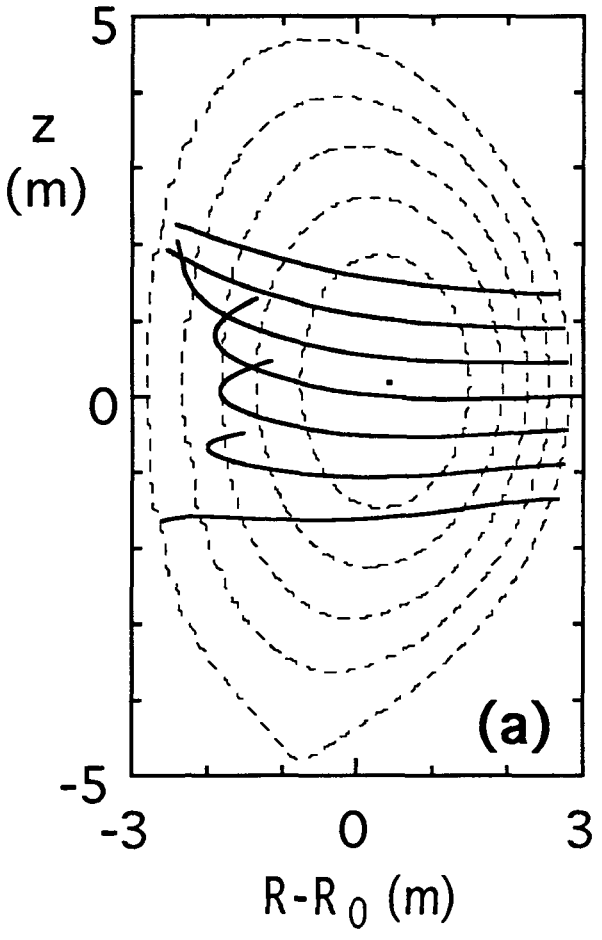

Fig. 5(a)

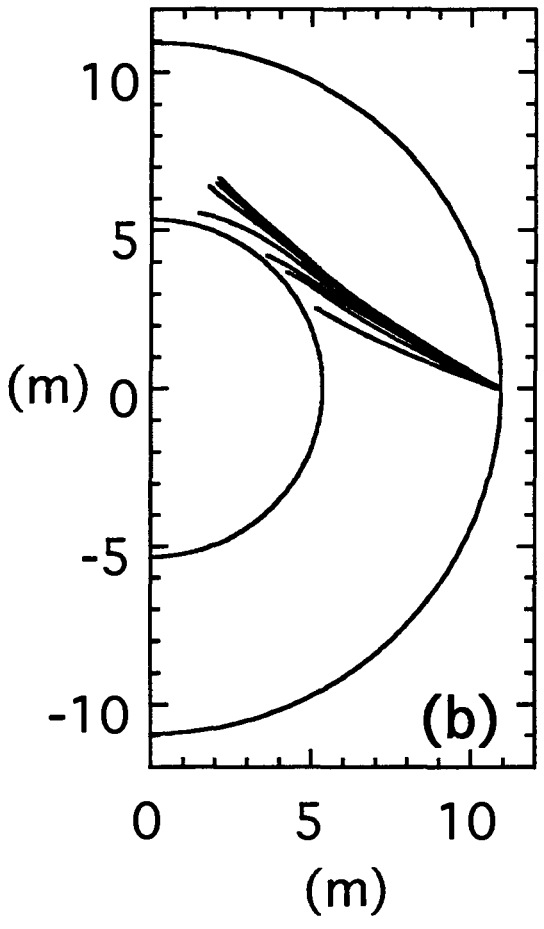

Fig. 5(b)

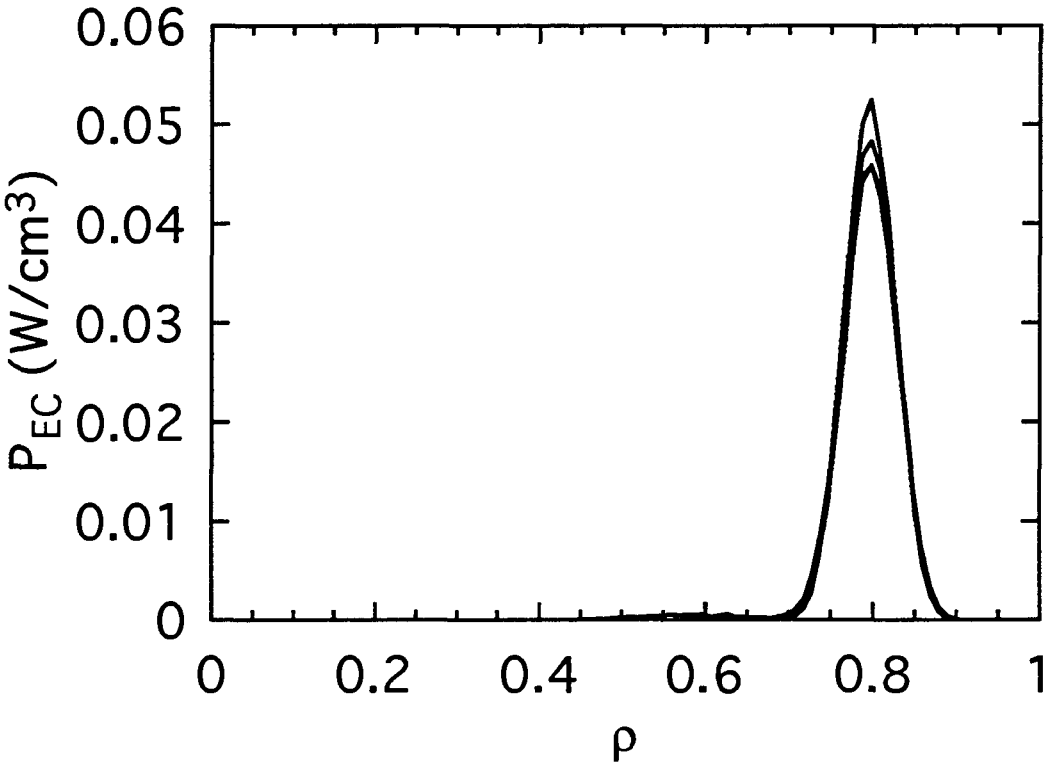

Fig. 6

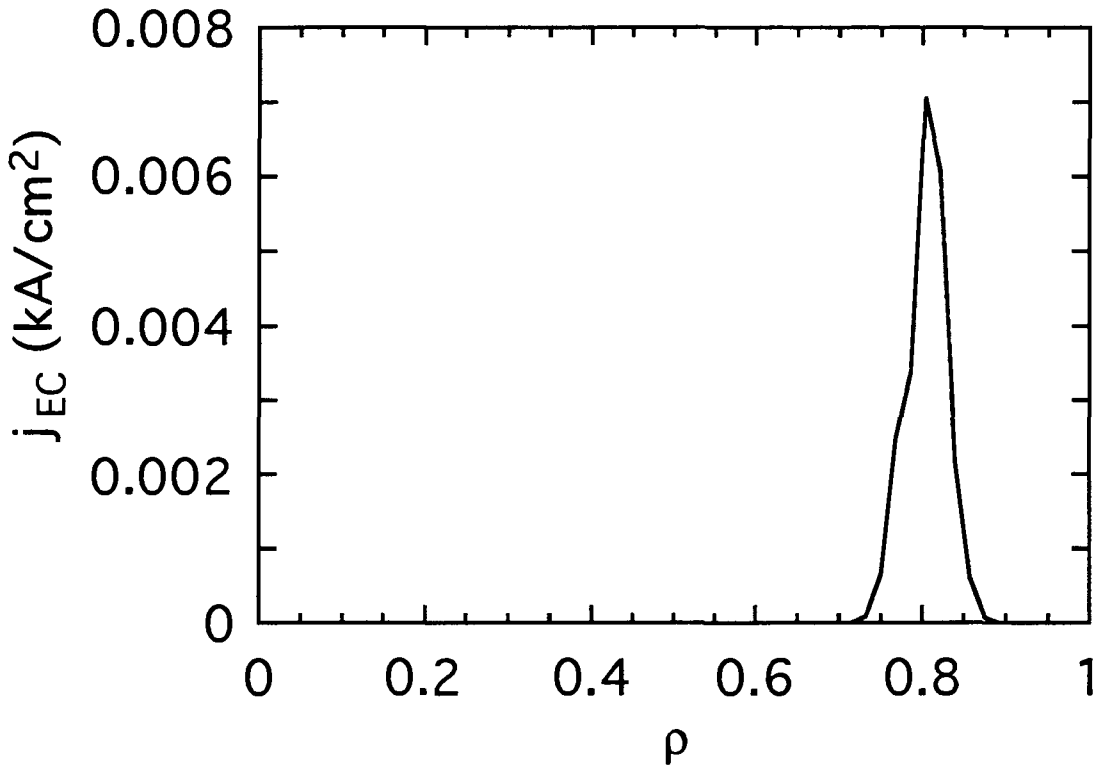

Fig. 7

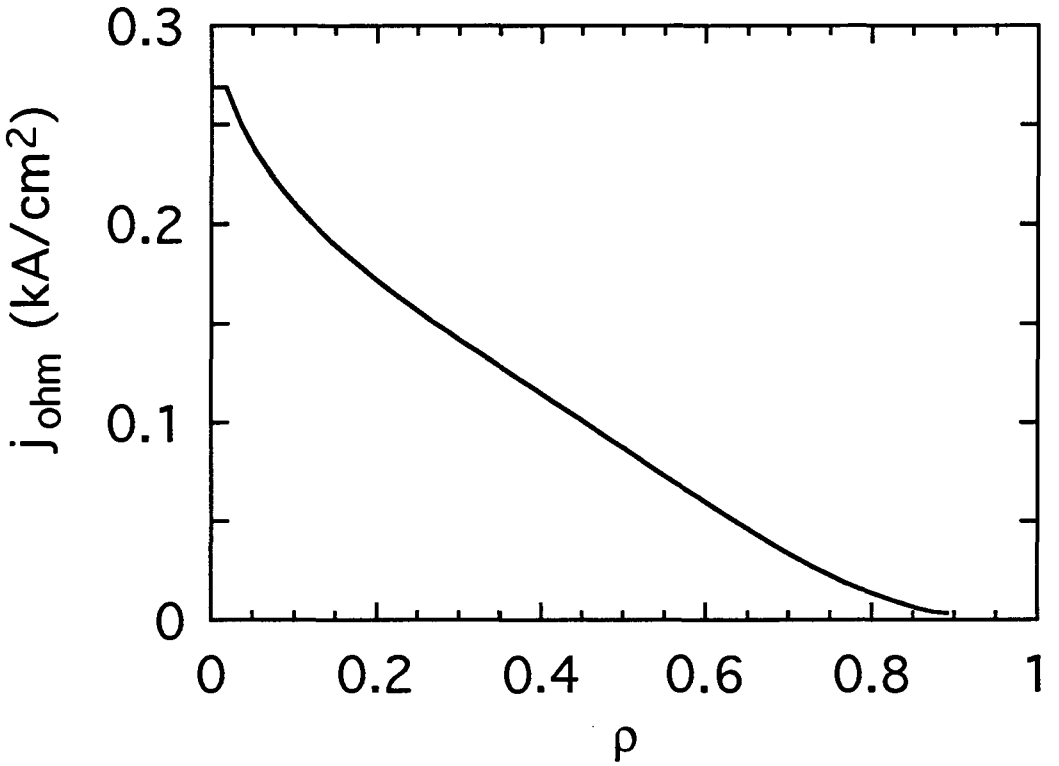

Fig. 8

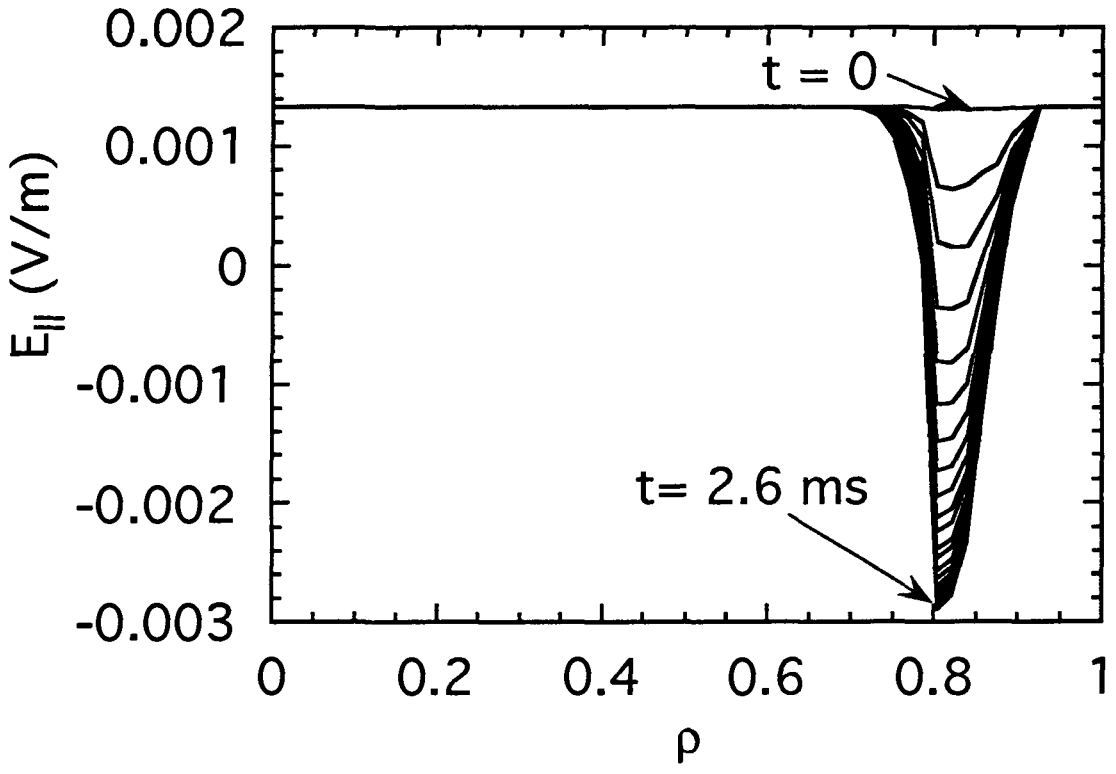

Fig. 9

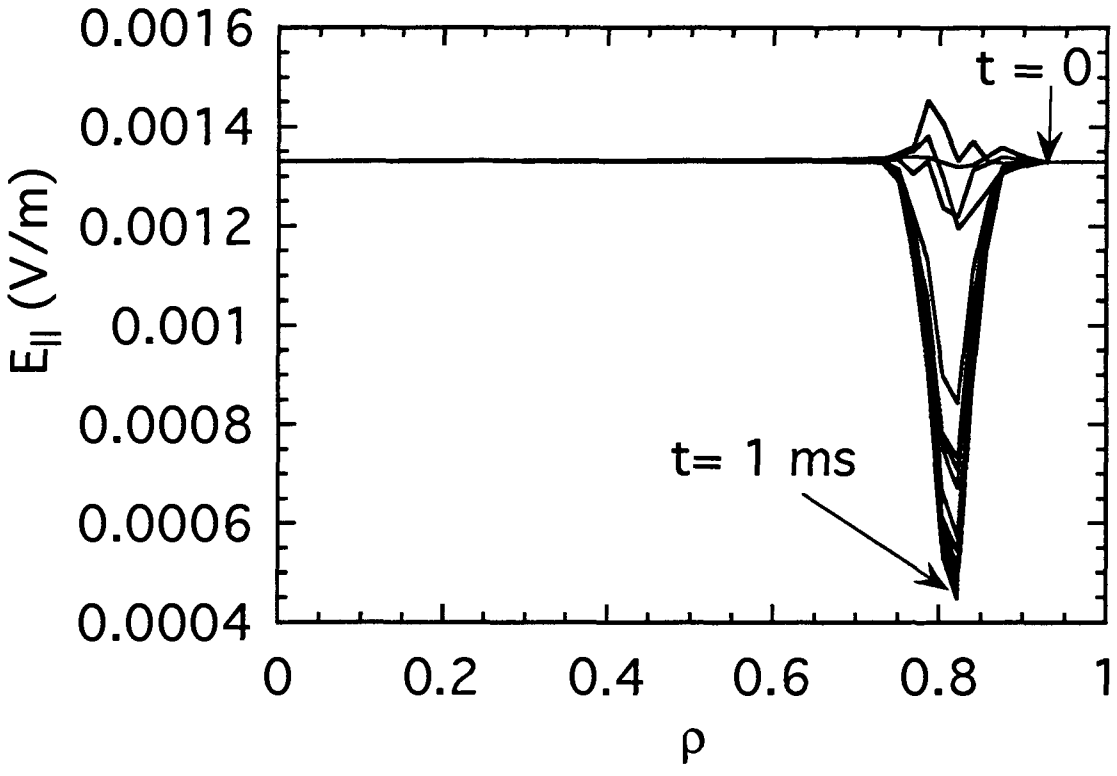
0.0016
0.0014
0.0012
0.001
0.0008
0.0006
0.0004
$E_{||}$ (V/m)
t = 0
t= 1 ms
0
0.2
0.4
0.6
0.8
1
ρ

Fig. 10

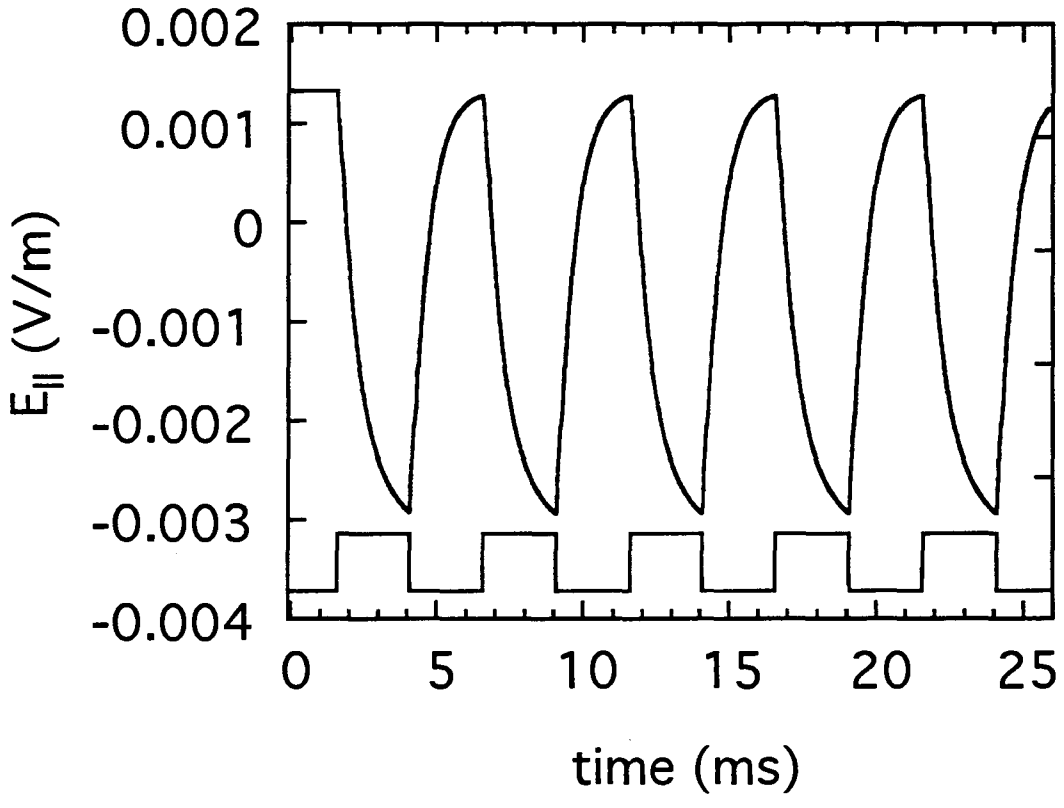

Fig. 11

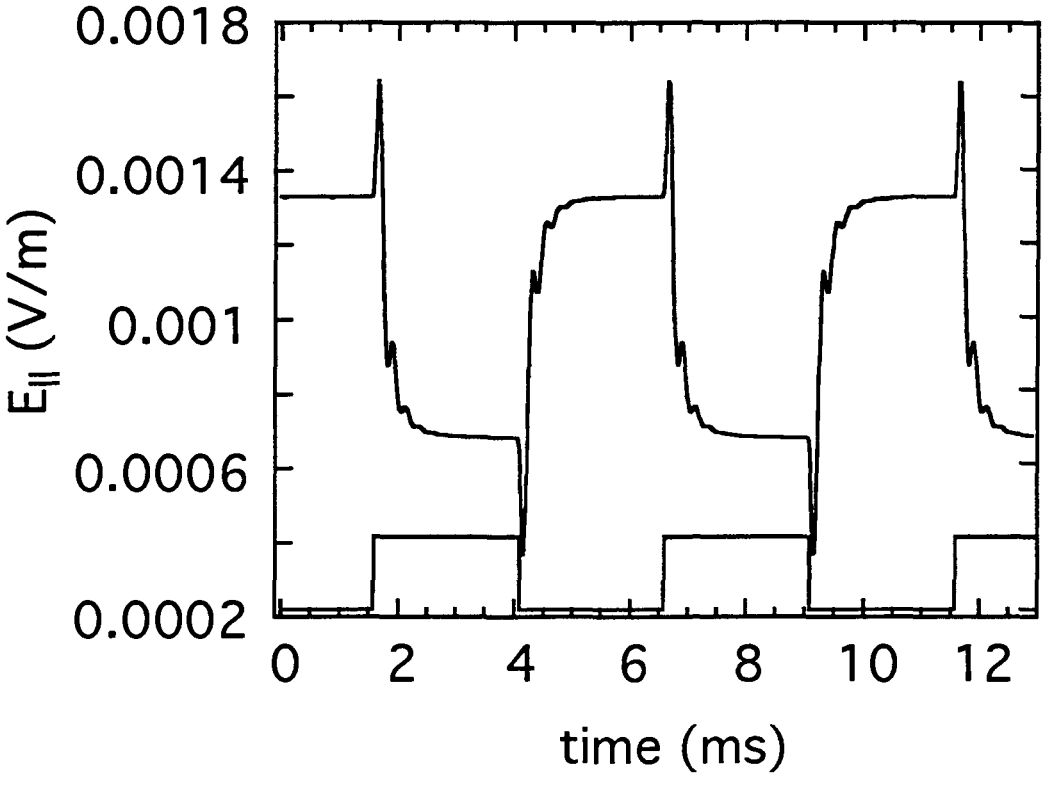

Fig. 12

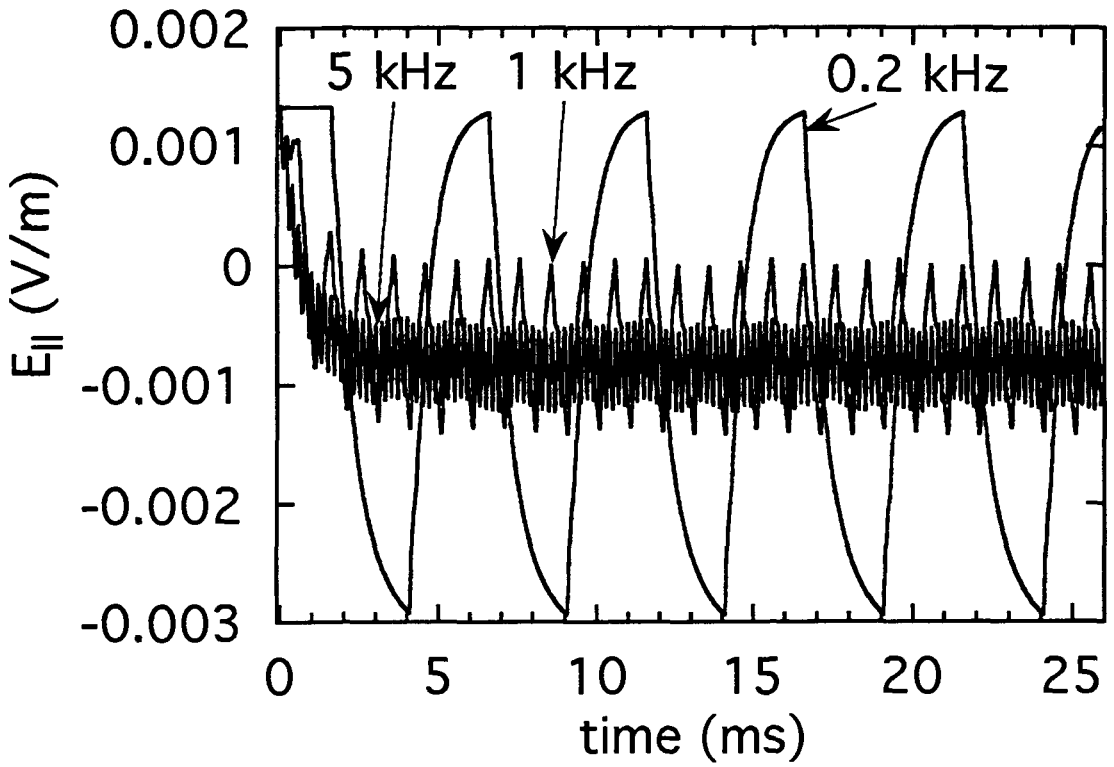
0.002
0.001
0
-0.001
-0.002
-0.003
$E_{||}$ (V/m)
5 kHz
1 kHz
0.2 kHz
0
5
10
15
20
25
time (ms)

Fig. 13

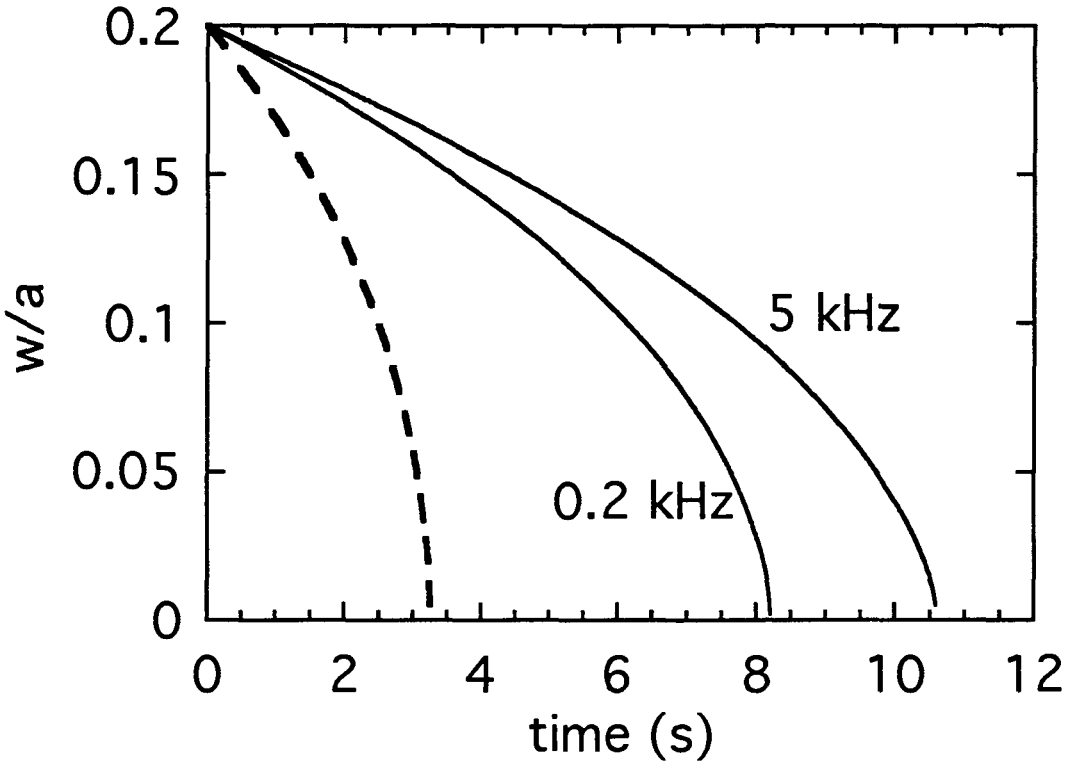

Fig. 14

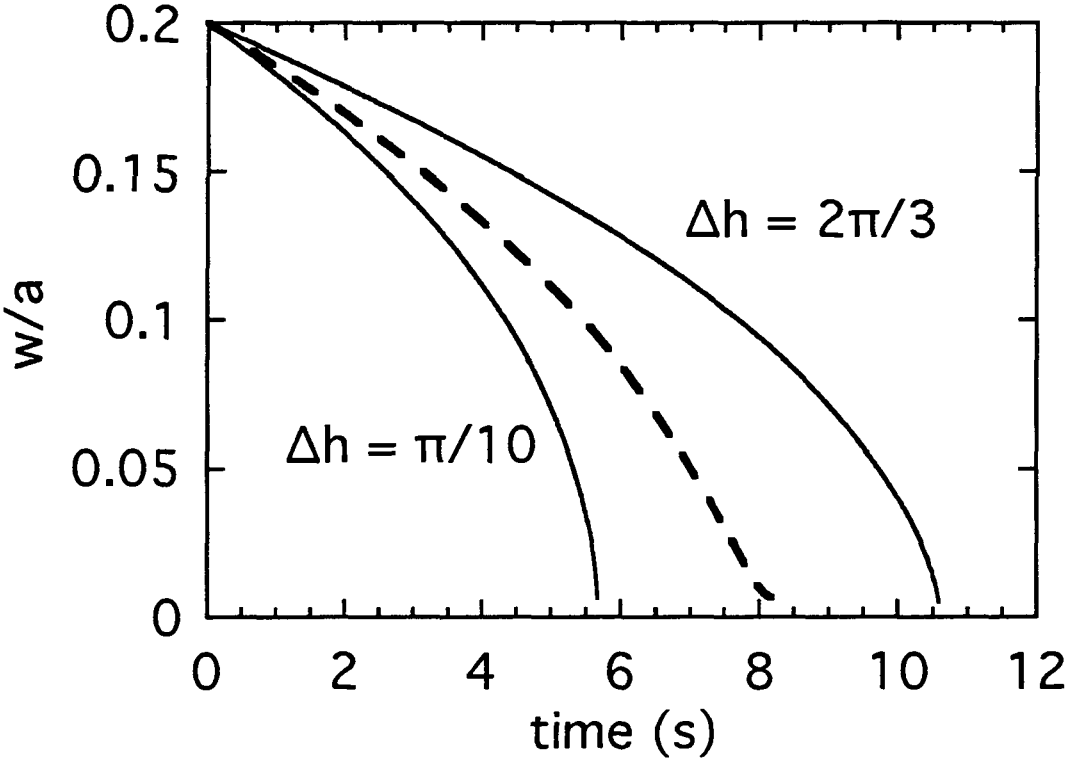

Fig. 15

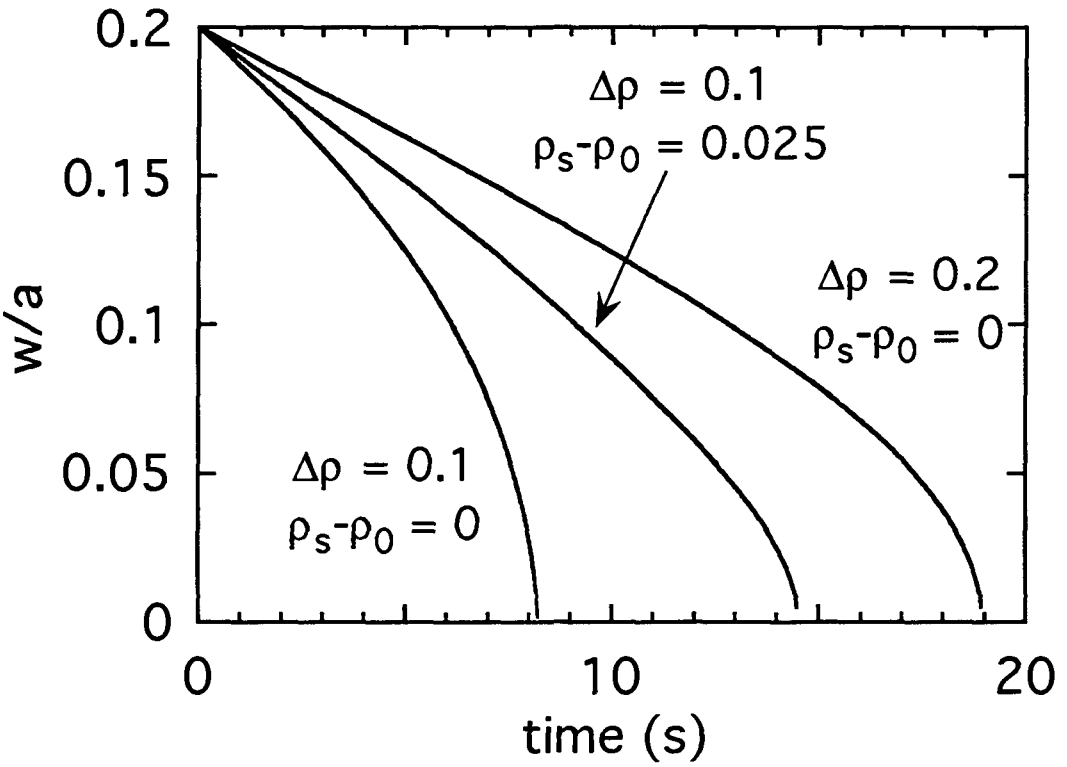
0.2
0.15
0.1
0.05
0
w/a
0
10
20
time (s)
Δρ = 0.1
ρs-ρ0 = 0.025
Δρ = 0.2
ρs-ρ0 = 0
Δρ = 0.1
ρs-ρ0 = 0

Fig. 16

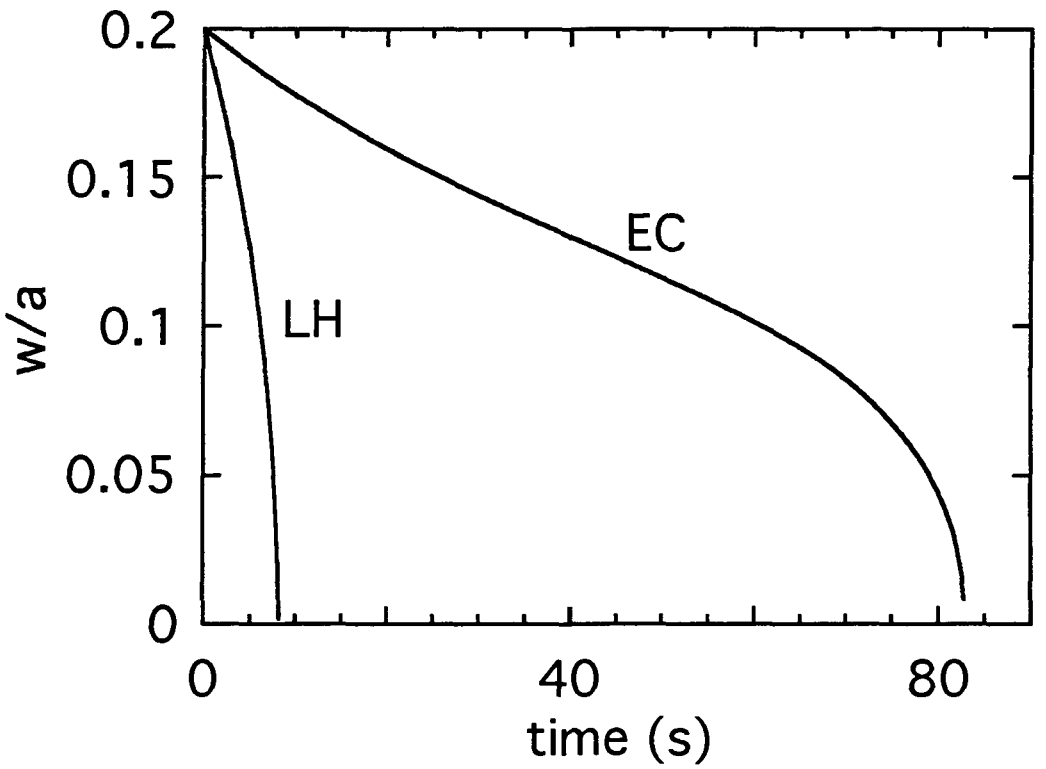

Fig. 17

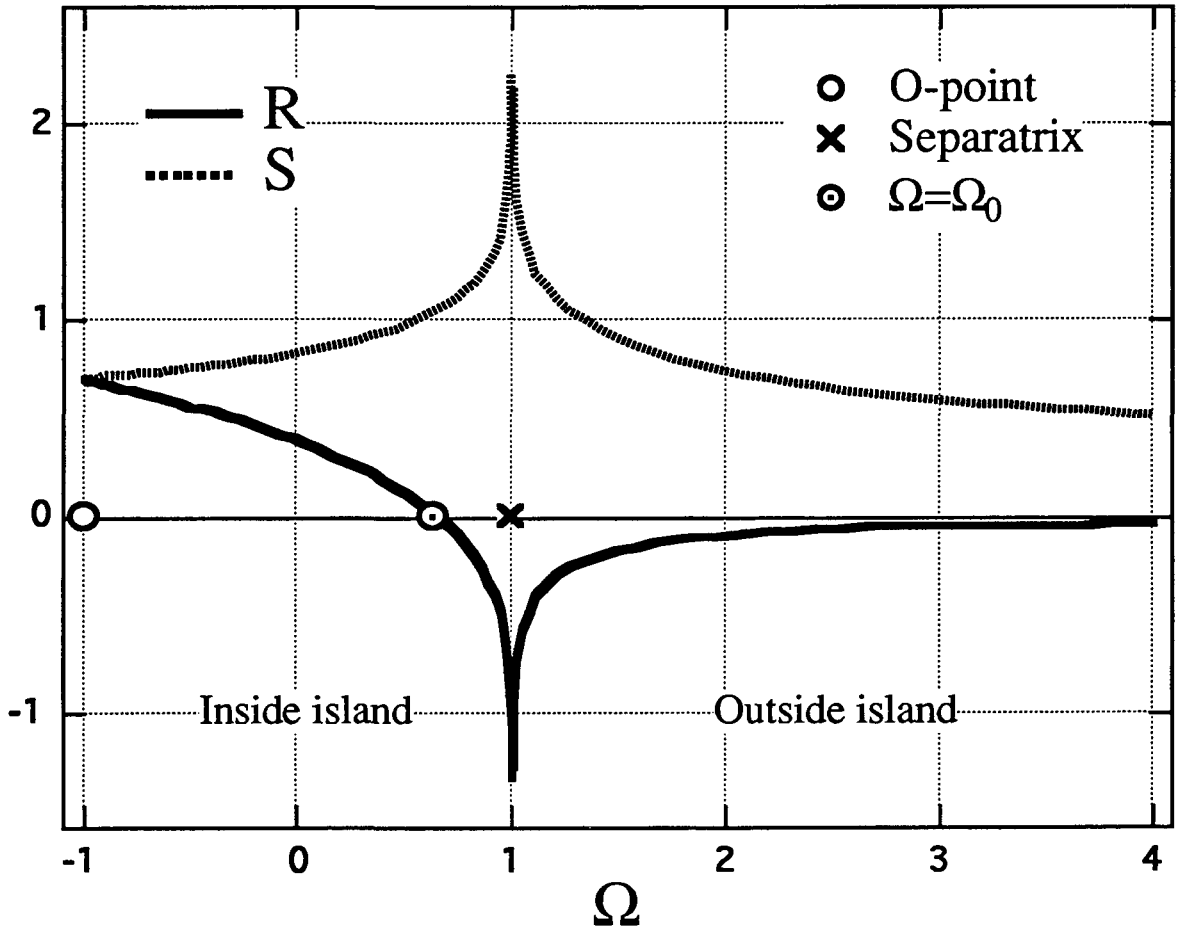

Figure A1

Functions R(Ω) and S(Ω).

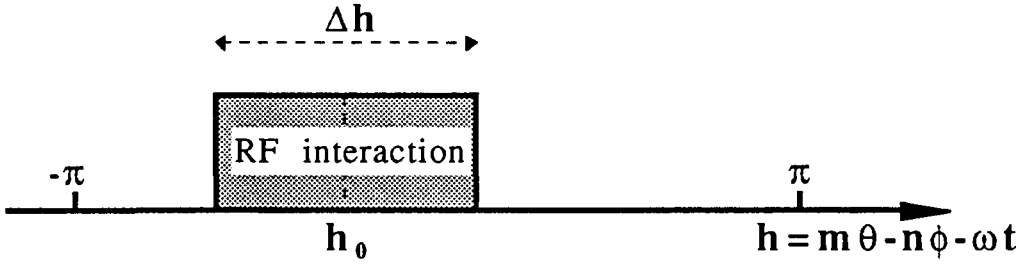

Figure B1

RF-interaction scheme.

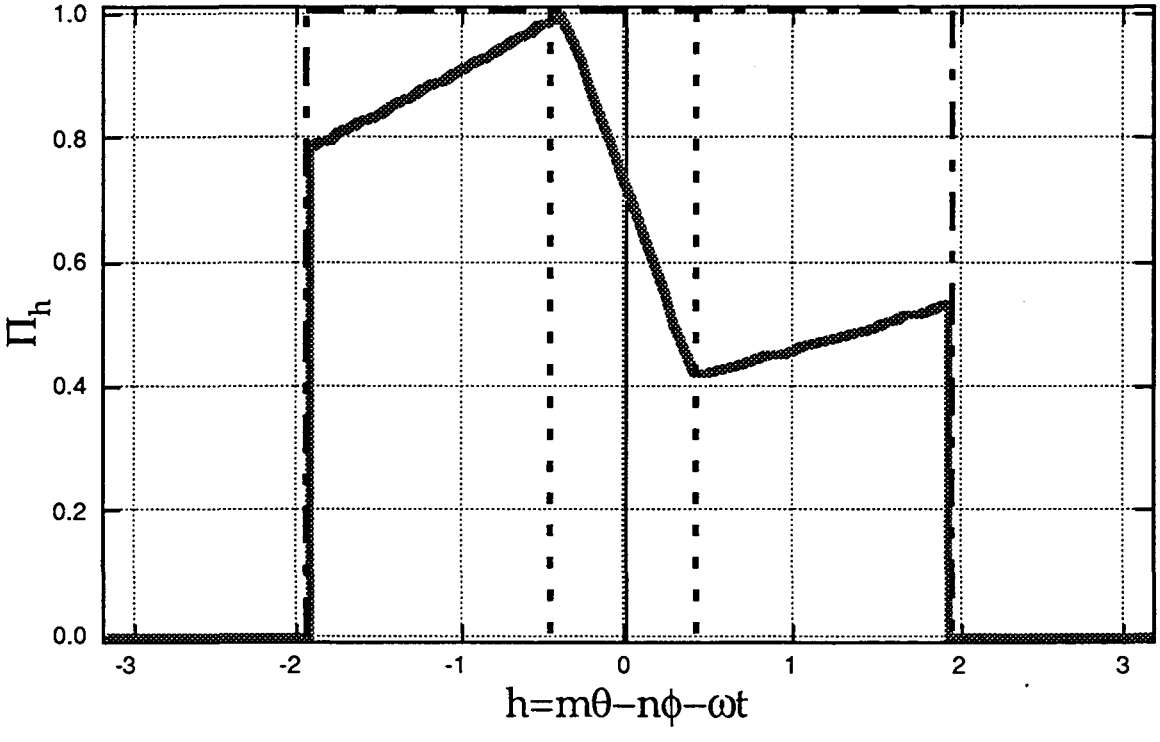

Figure B2

Various examples of the function Π_h, for $F_{on}=1/2$, $A_{on}=0$, $h_0=0$ and $\Delta h=\pi/4$:

$\omega\tau_c \ll 1$ (dashed line), $\omega\tau_c=1$ (continuous line)

and the case of reference [50] $\omega\tau_c \gg 1$ (dash-dotted line).